One Step Preparation of $BaFe_{12}O_{19}$/MWCNTs and Study of its Dielectric and Electrical Properties.

By

Zohaib Kamal

School of Chemical and Materials Engineering (SCME)

National University of Sciences and Technology (NUST)

2018

One Step Preparation of $BaFe_{12}O_{19}$/MWCNTs and Study of its Dielectric and Electrical Properties.

Name: Zohaib Kamal

Reg. No: NUST201463899MSCME67914F

This thesis is submitted as a partial fulfillment of the requirements for the degree of MS in Nanoscience and Engineering

Supervisor Name: Dr. Iftikhar Hussain Gul

School of Chemical and Materials Engineering (SCME)

National University of Sciences and Technology (NUST), H-12

Islamabad, Pakistan

Aug, 2018

THESIS ACEPTANCE CERTIFICATE

Certified that the final copy of MS/MPhil thesis written by Mr. Zohaib Kamal (Registration no. NUST201463899MSCME67914F), of School of Chemical & Materials Engineering (SCME) has been vetted by undersigned, found complete in all respect as per NUST fulfilment for award of MS/MPhil degree. It is further certified that necessary amendments as pointed out by GEC members of the scholar have also been incorporated in the said thesis.

Signature: _____

Name of Supervisor: **Dr.Iftikhar Hussain Gul**

Date: _____

Signature (HOD): _____

Date: _____

Signature (Dean/Principal): _____

Date: _____

Dedicated To

My Parents, Brothers and Sister.

Acknowledgment

With the blessing of all almighty Allah, the most charitable, forgiving and the creator of this beautiful world, today I am able to acknowledge after a fruitful completion of my research project. I also present my thanks in a modest and heartfelt way to the Prophet Muhammad (P.B.U.H) on behalf of which this universe exists. An inspirational messenger from Allah and great teacher who teach us the way of life and humanity.

I would like to thank my supervisor Dr. Iftikhar Hussain Gul, who showed his kind interest in carrying this project, give me his precious time for complete guidance and fruitful advices during the whole research period. I feel proud to be his student. I will be thankful to him for my whole life.

I specially acknowledge my co-supervisor Dr. Zakir Hussain. His generous advices are one of the key factor results in successfully completing this research work. I will always remember his kind support and corporation in my life.

I present my gratitude to my entire lab mates, class fellows for being so kind, humble and keeping friendly environment with me during the whole period of my stay in the lab especially Mr. Zarar Khan and Mr. Mehmood Khan for their back support and advices from start to end of this project and their help in learning all the related equipment in the lab. I think without their effort I will be unable to complete this work in time.

It will be great pleasure for me to acknowledge my parents, brothers, sister and specially my fiancée Ms. Tehreem who supported me at every stage of my life. Last but not the least I would like to thank "National University of Science and Technology (NUST)" who give me this opportunity to complete my Ms in nanoscience and engineering.

Zohaib Kamal

Abstract

Here in this work we have followed a chemical way of synthesis (Co-precipitation) to synthesize $BaFe_{12}O_{19}$ nanoparticles to study the variations occurred in its Electric and Dielectric properties in the presence of MWCNTs. These nanoparticles are decorated on the outer surface of MWCNTs with the help of Ultrasonication by using O-xylene as dispersing medium. By the help of ultrasonication 5 samples were prepared containing 0,1,2,3 and 5% MWCNTs.

XRD patterns revealed the formation of pure Hexaferrites phases of pure and decorated nanoparticles. The average crystallite size found for pure $BaFe_{12}O_{19}$ nanoparticles was 35nm. SEM shows the hexagonal, uniformly distributed homogenous nanoparticles grown by co-precipitation method. It also shows the successful attachment of nanoparticles on the outer surfaces of MWCNTs. FTIR results shows the absorption peaks for $BaFe_{12}O_{19}$ nanoparticles at 434.47,598.43 and 1431.80 cm^{-1}. A shift occurred in the absorption peaks of prepared composites ($BaFe_{12}O_{19}$/MWCNTs), which shows the successful attachment of $BaFe_{12}O_{19}$ on the outer surfaces of MWCNTs.

The dielectric parameters were studied in the frequency range of 1 MHz – 5 GHz. Dielectric constant (ε'), Dielectric loss (ε"), Dielectric loss tangent (tan δ) decreases with increase in frequency and increases with increase in wt% of MWCNTs in $BaFe_{12}O_{19}$/MWCNTs nanocomposites. The A.C conductivity is maximum at higher frequency which represent the dominance of hoping conductivity over band conductivity. The electric modulus increases with increase in frequency and decreases with increase in wt% of MWCNTs in $BaFe_{12}O_{19}$/MWCNTs nanocomposite. The Cole-Cole plot of electric modulus gives semi circles and relaxation time at higher frequencies. The impedance (Z) decreases with increase in frequency and also decreases with increase in wt% of MWCNTs in $BaFe_{12}O_{19}$/MWCNTs nanocomposite. The resistivity "lnρ" of the prepared samples was plotted against "$1/k_BT$" in the range 20 – 32 $(ev)^{-1}$. It represents decrease of resistivity with increase in temperature. The drift mobility(μ_d) shows maximum values at higher temperature and it increases with increase in wt% of MWCNTs in $BaFe_{12}O_{19}$/MWCNTs nanocomposite. These variations in the Electric and Dielectric properties of $BaFe_{12}O_{19}$ due to MWCNTs made it an important material for the electromagnetic devices.

Table of Contents

List of Figures

List of Tables

(Chapter 1)

Introduction

1.1 Nano Technology

NANO Technology is the science of today, it tightens its grip on all over the world. It consists of several disciplines of science like, Physics, Chemistry, Biology, solid states, material science etc. It has a lot of applications which are available in markets now days. Nanomaterials have totally different properties than bulk materials. The physical properties of a substance changes as we move from its bulk form to its Nano form. We can define Nano-materials as, those materials which have structured components with at least one dimension less than 100nm. On the basis of dimension structure, the Nano-material are categorized as 1-D, 2-D and 3-D. 1-D are those Nanomaterials whose one dimension is constrained only, examples of 1-D Nanomaterials are thin films and surface coatings. Its sizes can be varying in 2-dimensions, while its 3rd dimension will always have constrained less than 100nm. Similarly, in case of 2-D and 3-D Nanomaterials 2 and 3 dimensions will remain less than 100nm in its Nanoscale materials. For example, Nanotubes and Nanowires are 2-D Nanoscale materials in which two dimensions are always remain in the range of Nanoscale. Precipitates, collides and quantum dots are the examples of 3-D nanostructures. In case of these particles, all the three dimensions are constrained to nanoscale. Which means that all the three dimensions of a 3-D nanostructured material remain less than 100nm.

As the nanomaterials have different properties than its bulk counterpart. The main reasons which are responsible for their changes in properties on nanoscale are relative large surface area and quantum effect. These two reasons or properties of a material are responsible for the change of different material properties like electrical properties, strength and their reactivity. As we move from bulk to nanoscale, surface to volume ratio of a material increases which in the result enhances different properties like electrical properties and magnetic properties. We can tailor and control properties of a nanoscale material by controlling or tailoring its particle size. [1]

In nanotechnology, a new material is fabricated rather by handling different and new techniques (like a vast variety of techniques used for the fabrication of thin films) or in the result of self-assembly. Nanotechnology has already been given us a lot of new materials and new methods in almost all fields of science and yet more to be discovered. Those materials are very important and useful in those fields.

1.2 Magnetic materials and its Types

As an atom consists of several electrons which revolve around the nucleus in different orbits and spin around its own axis in clockwise direction or anticlockwise direction. In an atom, each electron produces its own magnetic field and if the magnetic field is applied to it externally, it responds to the external magnetic field in a specific way. According to law of electromagnetic induction proposed by Faraday "the magnetic force of electrons in a material is effected when the material is placed in a magnetic field". Thus, the materials which has a net magnetic field of its own originated from their atoms or dipoles and respond to the external applied magnetic field are known as magnetic materials. Magnetic materials are classified in different groups accordingly to their behavior when placed in a magnetic field, these groups are discussed below one by one.

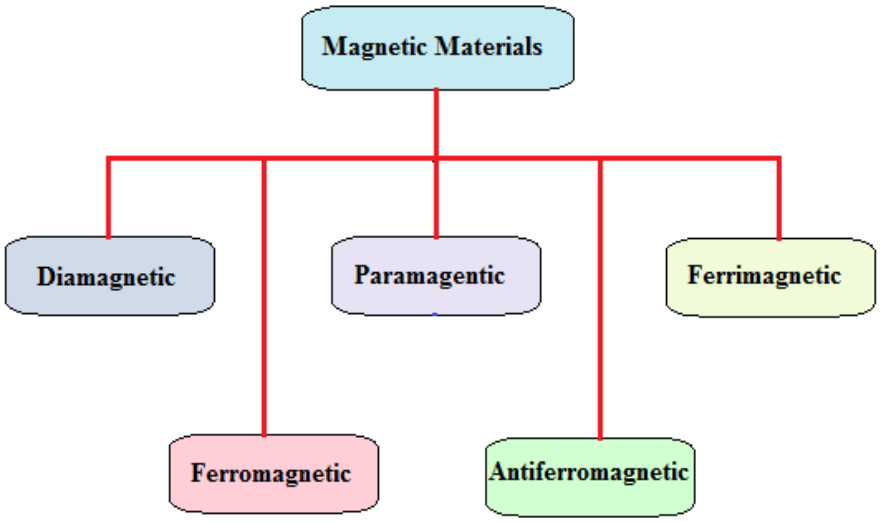

Fig.1.1 Types of magnetism.

1.2.1 Diamagnetic Materials

In diamagnetic materials, the magnetic moment is zero and thus has no internal magnetic interactions. In such type of materials, the external shells of their atoms are completely occupied. When diamagnetic materials are placed in the external magnetic field, the orbiting electrons are disturbed because of change occurs in its orbital angular momentum. The change in orbital angular momentum induces a magnetic moment in the diamagnetic material which always opposes the external applied magnetic field thus diamagnetic materials are opposes by external magnetic fields and thus having a negative susceptibility. Materials with filled shells and having even atomic number like N_2, H_e, H_2 and compounds like NaCl show diamagnetic properties.

1.2.2 Paramagnetic Materials

Paramagnetic materials show magnetization only in the presence of external magnetic field. Paramagnetic materials consist of permanent dipoles which are randomly oriented inside the magnetic materials if there is no external magnetic field. The dipoles are arranged randomly canceling the magnetic effect of each other and shows a zero-net magnetic effect on the material. When a paramagnetic material is placed in an external field, a torque is provided to the magnetic dipoles and they align themselves in a proper direction i.e. in parallel or in anti-parallel direction to the applied magnetic field and they get magnetized. But when the external magnetic field is removed then the aligned dipoles again loss their energy in no time and go back to their original random positions and shows no magnetic properties again. Paramagnetic materials have positive susceptibility because they are attracted towards the source which applied an external magnetic field unlike diamagnetic materials which have negative susceptibility.

1.2.3 Ferromagnetic Materials

Iron, rare-earth and actinide elements are known ferro magnets, the atomic magnetic moment of these elements are aligned in a common direction under a specific temperature which is known as curie temperature [2]. Ferro magnets also show magnetization in the absence of an external field. Like paramagnetic materials ferromagnetic materials have also a positive susceptibility and attracted by the external fields. When such material is placed in an external magnetic field under the curie

temperature, the atomic magnetic moment of all atoms aligns themselves towards the applied external field and when the field is removed the atomic magnetic moment remains in that direction and the material shows magnetization in the absence of external field. When the temperature increases from the curie temperature for a ferromagnetic material then it shows paramagnetic properties. The ferromagnetic material has high saturation magnetization because of rapid increase in magnetization even in the presence of weak external magnetic field. Elements from the periodic table like Fe, Co, Ni, Sr and Br show ferromagnetic nature.

1.2.4 Antiferromagnetic materials

Antiferromagnetic materials are like ferromagnetic materials. When this type of material is placed in a magnetic field, the atomic magnetic moment is aligned in antiparallel direction to the external magnetic field. In antiferromagnetic materials, atomic magnetic moment of each atom is in opposite direction to the adjacent atom unlike ferromagnetic material in which all atoms show atomic magnetic moment in unique direction. As the magnetic moments of these materials tends to align themselves in opposite direction to its adjacent atom, thus they cancel the effect of each other and show no magnetization external field is zero like paramagnetic materials.

1.2.5 Ferrimagnetic materials

In Ferrimagnetic materials is the type of magnetic material in which magnetic moments of all adjacent atoms are in opposite direction as it is in antiferromagnetic materials. The magnetic moments of adjacent atoms are opposite in direction but are not equal in magnitude unlike in case of antiferromagnetic materials in which the magnetic moments are opposite as well as equal in magnitude. Ferrimagnetic materials, under curie temperature hold spontaneous magnetization just like ferro-magnets and they loss their spontaneous magnetization as the temperature increases from curie temperature and have no magnetic order.

1.3 Ferrites

The oxide materials which containing Fe^{3+} as the main cationic component are known as Ferrites. A class of Ferrites having formula $MO.Fe_2O_3$, in which M is metal like Co, Ni, Pd, Sr, Ba, etc. Iron oxides are historical component which are known for millennia. In the past the use of oxide materials is as pigments for paints and they are also used as magnetic compass materials due to their magnetic nature. For the first time the magnetic north was located by using magnetic iron oxide [3].

These hard, brittle, ceramic-like nature and structure sensitive materials known as ferrites are most widely used material now a day. The Ferrites have much higher values of electrical resistances than metals [2]. After the synthetization of soft Ferrites by J.L. Snoek [4] the research on manufacturing of ferrites materials take a fast track and now the researchers can manufacture soft ferrites on a large scale for commercial applications. The storage of information, the processing of information and the generation and distribution of electric power are those main fields in which ferrites play a vital role. Their electrical resistivity, low eddy current losses are those properties due to which ferrites gain its importance in communication technology also [5].

After the arrival of nanotechnology, the application of ferrites grew and gain more attentions due to their enhanced properties in their nanoscale sizes. High-density recording media and biomedical like targeted drug delivery took the full benefit from the ferrites and nanotechnology [6]. The reduction in size of ferrites also brought some other applications and also open new avenues of application [7]. The nanotechnology also opens new ways to synthesize ferrites particles in powder form with homogenous particle sizes, the discovery of new ways for the preparation of ferrites particles also attain a great attention for the researchers [8-11]. In the beginning, ceramic method was the method of preparation for the ferrites particles. The ceramic method is the method in which the reaction of oxides, carbonates or other compounds occur, which if followed by the grinding and heating. As the particle size of initial materials is variable so the product is calcined in ceramic material for a relatively high temperature for well-mixing. But this method has some limitations, like due to high temperature the process of evaporation occurs which also evaporate some constituent materials like lithium (Li), which brings the chemical inhomogeneity in the final product [10]. There

is also another limitation which concerns with the large particle size and the low surface area of the final product [9]. Researchers found a way to overcome the limitations involved in ceramic method. They mix the constituents at their atomic or molecular level.

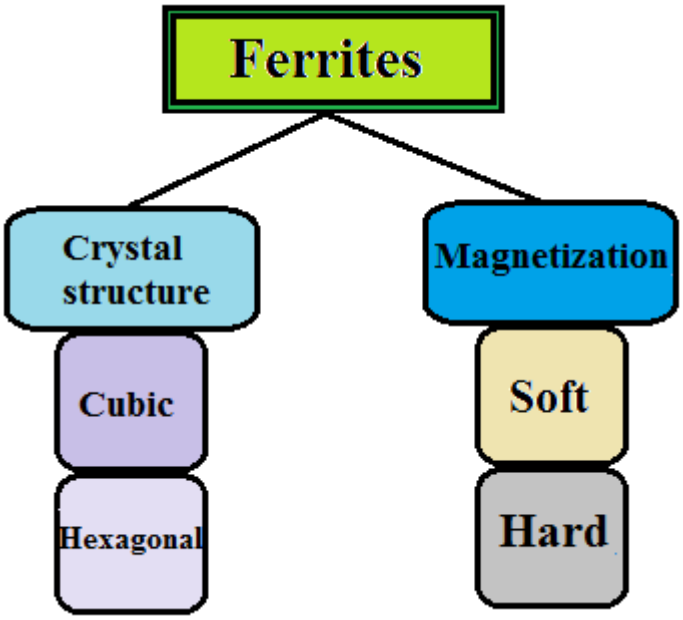

Fig 1.2 Classification of Ferrites based on their crystal structure and magnetization.

There are two ways to classify the ferrites, if we classify ferrites on the basis of crystal structure then they are classified into cubic and hexagonal ferrites and if we classify them on the basis of their magnetic behavior, then they can be classified into soft and hard ferrites [12]. The magnetization and demagnetization of soft ferrites can easily occur in the presence of magnetic field. In other properties of soft ferrites, their permeability is high where they have low coercivity their coercivity is always less than 1000 A/m and they have narrow hysteresis loop. Ferrites like $MnZnFe_2O_4$ and $NiZnFe_2O_4$ are the two examples of soft ferrites. Soft ferrites are used in many applications, power electronics circuits, inductors, small size antennas, chocks, volatile and nonvolatile memories etc. are some useful applications of soft ferrites. In contrast to soft ferrites, hard ferrites are act as permanent magnets. Their magnetization and demagnetization are not that easy as soft ferrites. Their permeability value is high, they have remnant magnetization, they have high coercivity which make them permanent magnets and have a wide hysteresis loop. The

ferrites with composition formula $MFe_{12}O_{19}$ are known as hard ferrites like $BaFe_{12}O_{19}$, $SrFe_{12}O_{19}$, $PdFe_{12}O_{19}$ and $CaFe_{12}O_{19}$. Hard ferrites have usually found in Hexagonal structure. Permanent magnets have a wide range of use in our daily life our houses, cars, electrical devices all contain permanent magnets. Hard ferrites are also used for purpose of high density storage and in audio and video tapes. These applications of hard and soft ferrites and their low costs make ferrites very useful candidate in the innovative applications [13].

Ferrites can be classified on the basis of their crystal structure too. On the basis of crystal structure, they can be divided into the following three types.

Type	Structure Formula	Example
Spinal Ferrites	$1Fe_2O_3 - 1MeO$ (MeO = transition metal oxide)	$MnZnFe_2O_4$, $NiFe_2O_4$, $CoFe_2O_4$, $MgFe_2O_4$ etc.
Garnets	$5Fe_2O_3 - 3Me_2O_3$ (Me_2O_3 = Rare metal Oxide)	$Y_3Fe_5O_{12}$, $Gd_3Fe_5O_{12}$ and $Dy_3Fe_5O_{12}$
Hexagonal Ferrites	$6Fe_2O_3 - 1MeO$ (MeO = group IIA oxide, e.g., CaO, BaO, SrO)	$SrFe_{12}O_{19}$, $BaFe_{12}O_{19}$ and $PbFe_{12}O_{19}$

Table 1.1 Classification of ferrites

1.3.1 Spinal Ferrites

Spinal Ferrites and Garnets are the subtypes of Cubic Ferrites. The structure for the spinal ferrites known as spinal structure is first discovered by Braggs and Nishikawa in 1915 [14]. Their high value of electrical resistivity and low eddy current are those properties which made the spinal ferrites the most broadly used family of ferrites. They have very excellent electrical and magnetic properties [14]. The spinal ferrites are further classified on the basis of their cations distribution on tetrahedral and octahedral sites. They are classified in the following groups.

- Normal spinal Ferrites
- Inverse Spinal Ferrites
- Mixed Spinal Ferrites

Spinal Ferrites are normally composed of trivalent and divalent ions. In normal spinal ferrites, the divalent ions attached to the tetrahedral sites where all the trivalent ions are found on the octahedral sites. In inverse spinal Ferrites, the trivalent ions occupy partial tetrahedral sites and partial octahedral sites and the remaining numbers of trivalent ions are distributed in the octahedral sites randomly. In third type of spinal ferrites which is "Mixed Spinal Ferrites" the octahedral and tetrahedral ion sites are filled by both trivalent and divalent ions. In case of mixed spinal ferrites, the number of trivalent and divalent ions on octahedral sites are unequal unlike inverse spinal ferrites in which half of the octahedral sited are filled by divalent ions and half by trivalent ions.

1.3.2 Hexagonal Ferrites

Hexagonal Ferrites have general formula $6Fe_2O_3 - 1MeO$, they got a lot of attention in practical applications due to their high coercivity. These materials are very important in the field of electronics and telecommunications. They are also used as permanent magnets and in high frequency microwaves devices [15]. Their hexagonal structure consists of two types of oxygen layers. The first layer is made of four oxygen ions where the second layer is made of three oxygen ions and the fourth site in this layer is occupied by barium ion. Besides these two layers there are also tetrahedral, octahedral and trigonal bipyramidal interstitial sites between the layers which are surrounded by four, six and five oxygen ions respectively [16]. Moreover, their hexagonal structure consists of further sub-units which are known as S, R and T and their rotationally symmetry (S^*, R^* and T^* respectively) around hexagonal c-axis at 180^o. The number of oxygen in all these sub-units is different. These basic blocks (S, R and T) classify the Hexagonal Ferrites in some other types. Which are given in Table 1.2.

Symbol	Chemical Formula	Unit Cell Structure	No of oxygen layers
M	$BaFe_{12}O_{19}$	RSR^*S^*	10
W (M+S)	$BaMe_2Fe_{16}O_{27}$	$RSSR^*S^*S^*$	14
Y	$Ba_2Me_2Fe_{12}O_{22}$	3(ST)	18
Z (M+Y)	$Ba_3Me_2Fe_{24}O_{41}$	$RSTSR^*S^*T^*S^*$	22
X (2M+S)	$Ba_2Me_2Fe_{28}O_{46}$	3 ($RSR^*S^*S^*$)	36
U (2M +Y)	$Ba_4Me_{12}Fe_{36}O_{60}$	$RSR^*S^*T^*S^*$	16

Table 1.2. Classification of Hexaferrites [17]

In table 1.2, in chemical formula column "Me" is a divalent cation and Ba Ba^{2+} ion which can be replaced by Ca^{2+}, Pd^{2+} or Sr^{2+} ions, because they have similar ionic radii to Ba^{2+} ion.

M-type Hexaferrites are one the most important group of hexaferrites which is used in different applications like in permanent magnets, due to their unique or important properties. They have high value of magnetization, they have high anisotropy and also they have high value of coercivity and these properties are making hexaferrites as most wanted material in high-density recording [18].

1.3.3 M-type hexaferrites and its crystal structure

The formula for M-type ferrites is given as $MFe_{12}O_{19}$, in which M can be replaced by Barium (Ba^{2+}), Strontium (Sr^{2+}) or Lead (Pb^{2+}). In case of subtituted ferrites Fe^{3+} is also replaceable by some trivalent ions or binary mixture of divalent and trivalent ions, but the replacement should not bring any distortion in the crystal structure of M-type ferrites. This replacement is done to obtain materials of different nature and tailored properties.

The unit cell of M-type ferrites is consisted of five layers of oxygen. Around the hexagonal axis crytal structure of M-type hexaferrites each molecule shows the rotation symmetry equal to 180^o. The oxygen layer which consist of M^{2+} act as a mirror plane, moreover this layer is also perpendicular to the c-axis. The unit cell of such ferrites is consisted of 10 layers of oxygen, which is composed of four further blocks i.e. S, R, S^* and R^*. S are spinal and R are hexagonal structures where S^* and R^* block are their mirror structures respectively which consists of atoms in similar arrangment to S and R but they are rotated at 180^o about the c-axis. Blocks S and S^* consists of two layers each of oxygen while their other counter parts i.e. R and R^* blocks consists of three layers of oxygen [13].

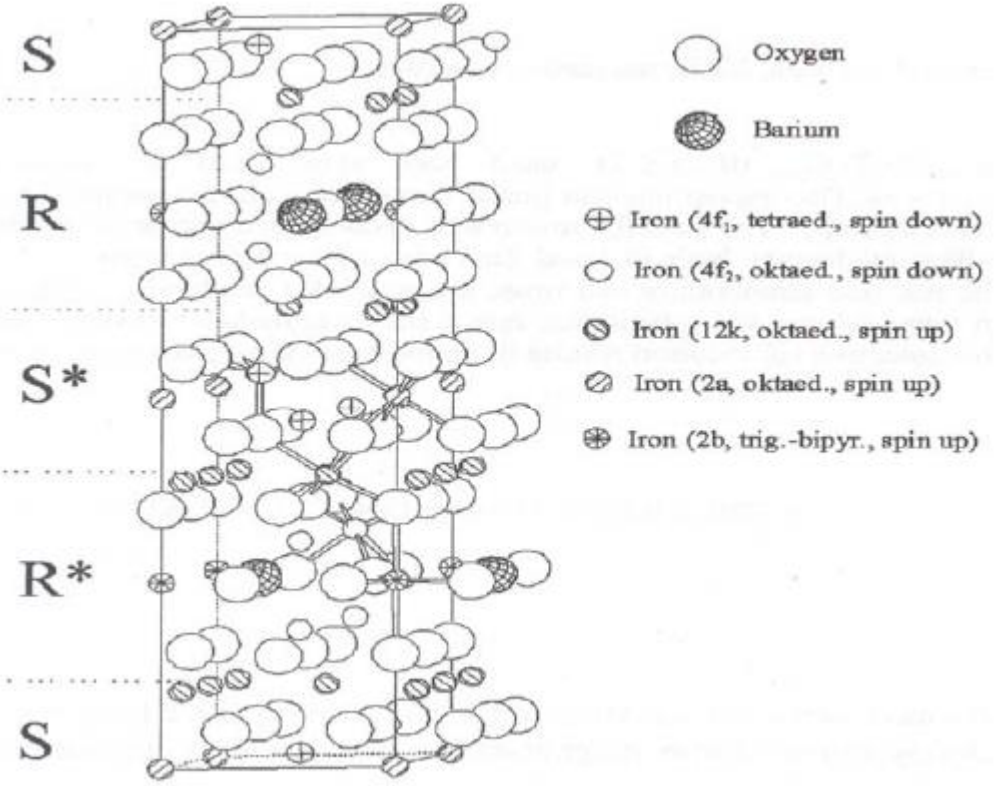

Fig 1.3 Two formula units M-type hexxaferrites crystal structure [17]

1.3.4 Applications of Hexaferrites

The hexaferrites are again on high preferences for past few decades due to their large number of applications. Hexaferrites have been used in different applications like magneto-optical storage and magnetic recordings [19]. Hexaferrite played a vital role in the miniaturization of divces, because such devices demands higher operating frequencies and power supplies and for the fulfilment of such demands the hexaferrites

have the desire properties in contrast of low budgets. Hexaferrites the magnetic dielectric have some properties like higher electrical resistvity (>10^6 ohm cm) which made them more promisable intetity for different applications as compare to other magnetic materials.

Hexaferrites are also used as core for transformers because they have high magitization, high electrical resistivity and low losses. Other very important devices like television receivers and surface mount devices are also taking benefits of the properties of hexaferrites. Moreover the recording heads for audio, data storage and video recordings are the applications of M-type hexafferites. The electronic industry contain a very large number of applications of hexafferites because they have high remanence, high magnitization, they are very stable and they are also cheap materials.

1.3.5 Strontium M-Hexaferrites

The reason behind the attraction of attention of researchers by strontium M-hexaferrites is the great potential of this material for applications. This material is applicable in the application due to its magnetocrystalline anisotropy, electrical resistivity, high saturation magnetization and low dielectric losses. Their magnetic bahavior is very well explained by magnetic moments of ferric ions and the strong exchange interaction. Some of the properties of such materials is explained below.

1.4 DC-electrical properties

There are three basic types of materials which are conductors (metals), insulators and semiconductors. They are catergeriozed on the basis of their tendency to carry electric charge. The materials which are good carrier of electric charges i.e. having higher conductivity have the lower activation energy. The insulators have very high activation energy. In case of some insultors and semiconductors their conductivity increases by increasing temperature but in case of metal a gradual decrease occurs in the conductivity of metals as we increase the temperature. Ferrites are strucure sensitive materials the conduction of electric charges in the ferrites depends upon the strucutre of the ferrites. The structure of ferrites can be changed by its synthesis route, amount of substituents, anealing temperature, reaction temperature, type of subsitunets etc.[20] As compared to metals, ferrites have high electrical

resistance and its electrical resistivity can be controlled or enhanced by the controlling the factors defined above [21].

By the electrical properties of a materials depends on the generation of the electric charges in the material and their transport inside the material. In ferrites the conduciton or transport of charge carriers occcur in the form of hopping which is explaind in the Verwey model [22]. The hoping of charge carriers in the ferrites occure between the ions at octahedral sites. The hopping depends on the seperation between the ions, for the conduction of charge in ferrites the charge carries must have overcome the potential barriers i.e. the charge carrier should have much energy to hope from one ion to another. That minimum energy which charge carrier required to overcome the potential barriers is known as activation energy [23]. The transportaion of charge carriers in M-type ferrite materials is also occurred by hopping thus they are hopping semiconductors or it is said to be small polaran hopping semicondutors having large number of mobile electrons [24]. The hopping of electrons ferrites occur between the Fe^{3+} and Fe^{2+} ions which are situated on octahedral sites [25]. This exchange can be different in different materials depending upon the orbital overlaping of Fe^{3+} and Fe^{2+} with oxygen [26].

1.5 Dielectric properties

Ferrites have high activation energy which indicates their high resistivity at room temperature. This property of ferrites make them suitable for applications as dielectric materials. The non-conducting materials are mainly used as dielectric materials, it is very informative to study the interaction of electric field with the atoms of dielectric materials. In dielectric materials polarization occurs when they are exposed to an electric field, the polarization results due to the occurance of induced dipole moments. When an electric field is applied the electron cloud move to one side resulting in the creation of dipoles which is characterized by its diapole moments. In dielectric material each atom creates its small field, and this field interact with the field which is applied from the outside [27]. That process in which the negative charged electron cloud and positive ions of atoms or molecules are seperated and then the dipole is oriented accordingly to the applied field or the seperation of charge carriers which occurs at the interfaces of grain-boundries in the result of applied electric field is known as electric polariztion [28].

Polarization is categerized in the following main four types.

- Electronic polarization
- Ionic or atomic polarization
- Diapolar polarization
- Interfacial or space-charge polarization

The electric polariztion is reffered to interfacial or space-charge polarization as it is related with the trapped and mobile charges. This type of polarization mainly occurs in the amorphous and polycrystalline materials because in such type of material charge carrier like electrons, holes and ions are traped on some sites and they get mobilize after getting some energy [29]. The mecahnism which is responsible for the transportation is defined by knowing the dielectric behaviour of a material. The most important property of a dielectric material is its permitivity or relative permetivity which generally defines the dielectric constant of a dielectric material.

The dielectric constant of a dielectric material depends upon the following factors.

- Frequency of alternating electric field
- Rate of change of time-varying field
- Chemical structure of dielectric material
- Imperfaction (defects) of the material
- Physical parameters like pressure temperature etc.

The dielectric constant and the frequency of the applied external field both depends on each other. The dielectric polarization fluctuate accordingly to the fluctuation of external field, but there is always a lag between them. If the fluctions of dielectric polarization does not follow the fluctuations of external field then the dielectric of that material decreases. In case of low frequency applied fields the polarization follows the fluctions of the field and hence in that case the dielectric constant remains almost constant. In case of high frequency applied fields the polarization can not follow the field and its dielectric constant decreases and at one stage when the frequency to very high value then the orientation polarization stops due to relaxation of dielectric materials. There are different limits of frequencies at which the different types of polarization (ionic, electronic etc.) stops. As the electric

resistivity of M-type hexaferrites are very high, dielectric constant and dielectric losses which make them a promising material for the applications of microwave absorptions.

1.6 Carbon Nanotubes and its properties

Carbon nanotubes were reported for the first time by S. Iijima in 1991 [30-32]. Carbon nanotubes have cylinderical shape which are formed from covelently bonded carbon atoms. The end of the cylinders may be capped or open, in case of capped carbon nanotubes the ends are made of hemi fullerences [30]. The carbon nanotubes may be single walled or multi-walled [33]. Single walled carbon nanotubes (SWCNTs) are actually graphene sheet rooled in cylinderical form and if there are more graphene sheet rolled over to form the cylinderical form then they are known as multiwalled carbon nanotubes (MWCNTs). The graphene sheets can be rolled in angle of orientation to form carbon nanotubes which is known is its chirality. The electrical properties of the CNTs depends upon the chirality i.e. CNTs having different chirality have different electrical properities.

The chirality and diameter of carbon nanotubes defines their nature that whethere the carbon nanotubes are metallic in nature or semiconducting. In conjugated aromatic system of carbon nanotubes three out of four valence electrons of carbon atoms form sigma bond between C-C while the fourth valence electron forming delocalized π-bond [34]. These π-electrons are the reason for the transportation of charges in the carbon nanotubes because they are weekly bonded. The carbon nanotubes i.e. SWCNTs shows metallic nature or high conductivity if there is not any seperation between the occupied π-states and empty π-states. If there is a narrow speration between the occupied π-states and empty π-states then the carbon nanotubes will be of semiconducting nature and if the gap between the above defined states is very wide then the CNTs will be insulators.

The multiwalled carbon nanotubes (MWCNTs) are different in properties from single walled carbon nanotubes (SWCNTs) [35]. There are a lot of strucutures of MWCNTs but the basic structure are Russian dolls and roll which are shown in the following fig1.4.

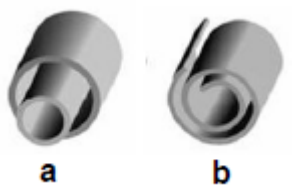

Fig 1.4. The models of the multi-walled CNTs **(a)** Russian dolls **(b)** roll

As the numbers of outer walls of MWCNTs are not fixed and by increasing number of walls, the shape of MWCNTs may not be cylinderical. It is also possible and seen in different cases that the nanotube shape changed into polyhedrons. There is also possibility of the formation of pentagons and heptagons on the outer walls of the MWCNTs which are then counted in the defects of the MWCNTs and curved and spiral carbon nanotubes are also formed in the result of these defects [34].

Carbon nanotubes are mainly used in different application due to their electrical, mechanical and thermal properties. These properties are explained below.

1.6.1 Mechanical properties of CNTs

As in carbon nanotube three out of four carbon valence electrons are involed in C-C σ-bond. The presence of these bonds in the carbon nanotubes made them mechanicaly very suitable in different applications. Theoritcally due to presence of C-C bonds it should be the stiffer substance known [36]. Theoritcal values for the Young's modulus was found to be 2.8-3.6 TPa and 1.7-2.4 TPa for SWCNTs and MWCNTs respectively where the experimetaly reported values for their Young's Modulus are 1470 GPa and 950 GPa [37, 38] respectivley. Due to their useful mechanical properties they are used in the following mechanical applications.

- Polymer fibres
- Aircrafts parts
- Sports goods
- Adhasives
- Mirror housings
- Car body panels

1.6.2 Electrical Properties of CNTs

Carbon nanotube are one diamenional (1D) structural material which is made of graphene sheets. Graphene have novel electrical properties and these electrical properties are enhanced when they are rolled in cylinderical shapes because in case of 1D structural materials the conducting electrons can not be scattered easily as it is possible in case of 3D structure materials. The theortical values for metalic SWCNTs are 10^5 to 10^6 S/m and 4×10^9 A/cm^2 for their conductance and currrent density respectively [36]. The conduction of electrical charges in MWCNTs depends upon the inner diammeter of the MWCNTs and the helicities of the outermost shell and also on the defects found on the outermost shell[39]. Theoritical values for MWCNTs have been reported for their conductivity is between 20 and 2×10^7 S/m [40]. The application in which carbon nanotubes are used to enhanced the electrical properties are given below.

- Fuel filler caps
- Automotive fuel lines
- Fuel filter housings
- Fuel hoses
- IC trays, carrier tapes
- Intermediate container
- Coatings
- EMI protection housings
- Mobile phones jammers
- Satellite navigations systems

1.6.3 Thermal properties of CNTs

Carbon nanotubes are also very good thermal conductors, as CNTs are in cylinderical shapes thus the heat can transfer through it in two ways i.e. across tube axis and along the tube. It is found from the literature that CNTs are thermaly good conductor along the tube and also along the tube axis [36]. It is very difficult to study the conductivity of a single tube but the according to the measurments SWCNTs has a thermal conductivity along its axis equal to ~3500 W m^{-1} K^{-1} where MWCNTs shows thermal conductivity equal to ~300 W m^{-1} K^{-1} [41].

Some of the applications in which carbon nanotubes are used due to their thermal properties are:

- Thermal management applications as heat pipes
- As metallic addition to low thermal conductive materials
- For the preparation of highly conductive electronic components
- For the preperation of Elastomers.

Some of the key potential applications are mentioned in Table 1.3 for MWCNTs on the short, mid and long-term.

Current/ Short-term	Mid- term	Long-term
Conductive polymers & composites (automobiles and electronics)	Coatings (conductive thin films)	Microwaves antennas
Sensors and instruments (microscope probe tips, gas leak detectors)	Catalysts (petrochemical)	Self-assembling yams
Electromagnetic shielding Sporting goods(tennis rackets)	Textiles and fibres	Aerospace
	Lithium ion batteries	Medical implants
	Memebranes and filters Lamps	Drug delivery
	Semiconducting Materials	
	Advanced ceramics	
	Fuel cells	
	Caulks and sealants	

Table 1.3. Applications of MWCNTs in short, mid and long terms

1.7 Literature study of Hexaferrites

Barium Hexa ferrites ($BaFe_{12}O_{19}$) were prepared by Radwan et al [42] with the help of coprecipitation-calcination process. In the process they used barium and feric chloride as their initial precursor and then by the use of hydroxide solution they precipitate the barium and iron ions. The pH value of the solution was 10 at room temperature. The calcination temperature for the calcination of the precursors was 800-1200^{o}C for for 2h. The magnetic properties of the produced ferrites particles was studied. They found that the number of formation of single-phase $BaFe_{12}O_{19}$ nanoparticles increases as they increase the calcination temperature. One can also achieve the uni-phase $BaFe_{12}O_{19}$ poweder by the help of decreasing the mole ratio

Fe^{3+}/Ba^{2+}. They reported magnetic saturation as 50.02 emu/g and intrinsic coervivities as 624.4 – 4580 Oe.

The coprecipetation method was also used by Iqbal et al. [26] for the preperation of Al-Ga substituted strontium hexaferrites. The composition of hexaferrites was $SrAl_xGa_xFe_{12-2x}O_{19}$ (x = 0.0–0.8). XRD technique was used for the confirmation of single phase of nanoparticles. The EDX technique was used for knowing about the elemental composition of the product, they also measured the DC electric resistivity by varying the temperature, they temperature range was 300 – 675 K. They reported the increase in the resistivity by increasing the Al-Ga content. The resistivity data was also used for the calculation of activation energy and drift mobility. The frequency range for the calculation of dielectric constant (ϵ) and dielectric loss (tan d) was 80 Hz – 1 MHz. They calculated the magnetic properties of their sample like saturation magnitization (Ms) and coercity (Hc) etc from the hyteresis loop. They found a decrease in the values of different parameters like dielectric constant, dielectric loss, saturation magnetization, remanence and coercivity with increase in Al-Ga concentration.

Zr-Cd substituted strontium hexaferrites were prepared by Ashiq et al. [43] with composition $SrZr_xCd_xFe_{12-2x}O_{19}$ (for x = 0.0–0.6) by chemical co-precipetation method. XRD technique was use for the phase detection, the magnetic properties were studied by analysis of their hysterisis loop where the dielectric properties were studied with the help of LCR meter. The crystallite size, lattice parameters and cell volume was obtained from the XRD data. They report the crystallite size of their ferrites in the range of 28-39 nm. The values of saturation magnetization increases by increasing the value of x from x = 0.0 – 0.2, the other magnetic parameters like remanence and coercivity showed a decrease in their values with increase in Zr-Cd concentration. The dielectric properties were measured in the frequency range of 500 Hz – 1 Mhz. The reported values of dielectric constant and dielectric loss were 3347–30 and 11–0.24 respectively.

Javed et al. [44] prepared Ca subtituted strontium hexaferrites with composition $Ca_xSr_{1-x}Fe_{12}O_{19}$ (x = 0.0-0.6) by co-precipitation method. The phase analysis was done with the help of XRD techinuque which showed the single magnetoplumbite phase containing calcium content. The EDX analysis was used to

optimize Fe/Sr ratio which was found to be 11. The drift mobility was derived which was increasing with decrease in resistivity. The decrease was occuring in the dielectric constant and dielectric loss as the frequency increases which shows its promisable future in microwave devices.

Ali et al. [45] prepared a magnetic nanocomposite from the composition of strontium ferrites thin films and MWCNTs. Nanoferrites with composition $SrFe_{10}(Sn_{0.5}Zn_{0.5})_2O_{19}$ were prepared by sol-gel process. The Ferrite/MWCNTs nanocomposite was prepared by ultrsonication process. The diameter of MWCNTs used in the composite was found from the TEM micrographs which was in the range of 70-80 nm. The formation of Ferrites/MWCNTs nanocomposite was confirmed from the XRD pattern which showed the ferrites peak at (1 0 7) and (1 1 4) where the CNTs peak was located at (0 0 2). The magnetic properties of the composite was studied by VSM techinque. The saturation magnetization and coercivity decreased as the quantity of nanotubes was increased. The magnetic properties showed applicability and usefulness of the that ferrite/MWCNTs nanocomposite in microwaves and electromagnetic absorbing fields.

Majid et al. [46] decorated Mn-Sn-Ti substituted strontium ferrites on the outer surface of MWCNTs in different volume fractions (10,15,20,25 and 30%). The strontium ferrites were prepared by Sol-gel procress and the decoration of the nanoferrites over the outer surface of MWCNTs was carried out with the help of ultrsonication. The phase analysis was carried out with the help of XRD technique. The morphological studied was carried out by studying their Field emission scanning electron microscopic (FESEM) pictures. FTIR study was alos carried out to study the nanocomposites. The magnetic properites of the composite were studied with the help of VSM and for microwaves absoption properties Vector newtwork analysis (VNA) analysis was performed. The VSM technique revealed that the saturation magnetization and the coercivity values of the nanocompostie decreases by increasing the MWCNTs content. The reflection loss found from the VNA was increased by increasing the MWCNTs content in the composite. The reflection loss value for the composite with 10 vol% MWCNTs was -15.1 dB and for 30 vol% MWCNTs this value increased to -28 dB.

(Chapter 2)

Synthesis of Ferrites Nano particles and the Composites

2.1 Methods of preparation

As the ferrites are very useful in different applications as discussed in their nanosize. The researchers discovered a lot of methods which are used to prepare hexaferrites nanoparticles.

Different methods which are used to prepare Hexaferrite nanoparticles are listed below.

- Co-precipetation
- Sol-gel
- Hydrothermal
- Mcroemulsion
- Spray-pyrolisis
- Citrate precursore method
- Reverse micelles method
- Sonochemical method

The sol-gel technique [47] is consist of two steps of alkoxide based precursore. These two steps are hydrolysis and condensation. In sol-gel a liquid solution is prepared from the initial material and then a solid gel is obtianed from that liquid by using a chelating agent, then this solid gel is converted into required product by the process of anealing. In this method the size of particles depeneds upon the composition of sol, its pH and the temperature on which the reaction is carried out. This technique consits of a number of different steps. The temperature provide in solgel for the purpose of anealing is not that much high but it required a lot of time for its completion. Moreovere the chelating agent used for gel formation, is also become a reason for the presence of impurities in the product.

Microemulsion method [48] is used to obtain very small size nanoparticles. In this method an emulsion is prepared from two solution, in which one is water-material solution and the other is oil-material solution. Then in the emulsion the reaction is carried out on a small scale by the help of a surfactant. Different surfactants (like Cetyltrimethylammonium chloride (CTAC) [49] and sodium dodecyl sulfate (SDS) [48] have been used by the researchers in microemulsion method to synthesize Hexaferrite nanoparticles at very small scale. The microemulsion method is very costly as compared to other methods, it requires large quantity of liquids and also the annealing temperature is very high.

Spray-pyrolisis method [50] is used to obtain the nanoparticles of high purity. In this method a soulution, suspension or sol is used for the production of aerosol droplets by the process of atomization. A microporous particle is obtained after the evaporation and drying of aerosold droplet. Then this microporous droplet is converted into a dense particle by the process of thermolysis which require high temperature treatment. The product obtained in the result of spray-pyrolisis is of high density but this method required a lot expanses to obtain such purity.

2.1.1 Co-precipetation method

Coprecipetation is a chemical wet method in which fine nanoparticle is obtained, it is also used for the prepration of fine, pure and homogenous nanoparticles of ferrites [51]. In coprecipeation method the nucleation, growth and agglomeration of nanoparticle occurs simultaneously. The first phase in coprecipetaion is the nucleation phase in which the precipetate forms of small particles. But the particles formed in the result of nucleation are of very small size and they are thermodynamically unstable, to gain staibality they aggregate togther to form thermodynamillcally stable large particles. This aggreation is called growth. The growth rate is slower than the nucleation rate. Therefore to obtain homogenious particle size nanoparticles in the producte the nucleation of the species present in the solution must be occur at the same time [52]. After the nucleation and growth of nanoparticles a basis solution like sodium hydroxide is added to the solution which helps in the precipetation of metal hydroxides. This this precipetate is washed and filltered to remove the metalic base which was added for precipetation purpose. After washing the resultant product is dryied and then annealed to obtain the desired mixed

oxide product [52]. It is a very simple method in which the proper mixing of precursors or metallic ions occurs due to which the final product consists of homogenous and small sized particles. The yeild of product is also high in coprecipetation method as compare to other methods and it is also a reliable and repreducible method for the preperation of ferrites.

2.2 Chemical Used

The first step in our work as to prepere the sample of high purity, for which we used different chemical which were in their highly pured forms and purchased from the well known suppliers. The details of the chemicals used in our research are given in Table 2.1.

S.No	Compound	Chemical Formula	Purity	Supplier
1	Barium Nitrate	$Ba(NO_3)_2$	99.0%	Aldrich
2	Sodium Hydroxide	NaOH	99.0%	Merck
3	Iron nitrate	$Fe(NO_3)_3 . 9H_2O$	99.0%	Merck
4	Ortho-xylene			

Table 2.1 List of chemicals used for the preparation of MWCNTs/$BaFe_{12}O_{19}$ samples

2.3 Sample preperation

The Barium hexaferrite having compositional formula $BaFe_{12}O_{19}$ was prepared by a chemical co-precipetaion method. In this process first of all the stiochiometric amount of $Fe(NO_3)_3.9H_2O$, $Ba(NO_3)_2$ and NaOH were dissolved in double dislled water in separate beakers with the help of magnetic stirring. After obtaining crystal solutions, the crystal solution of $Ba(NO_3)_2$ is mixed with $Fe(NO_3)_3 .9H_2O$ and again stirred for another 15 minutes. After that the temperature was increased to 80^oC of the mixed solution and stirred vigourusly and kept at that temperature for 15 minutes. After 15 minutes the crystal solution of NaOH at the same temperature was also mixed to $Ba(NO_3)_2$ and $Fe(NO_3)_3 .9H_2O$ solution and a mixed solution was obtained having

pH value equal to 12. Then the solution was kept at 80°C for another 30 minutes and stirred virgorusly the pH was kept at 12-13 pH value. After 30 minutes, the heating was turned off but the stirring was kept ON for another 4 hours.

In the result of above procedure a dark brown coloured solution was obtained which was then washed several times with double disttled water until the ph value 7 was obtained. After washing the sample was kept in oven for overnight drying on 90°C. Then the obtained product was crushed by motar and pestle and converted into a fine powder. Then the poweder was kept in a muffle furnace for 6 hours at 1100°C for annealing. After annealing the final product was again crushed into fine powder. Following is the schmatic for the whole process.

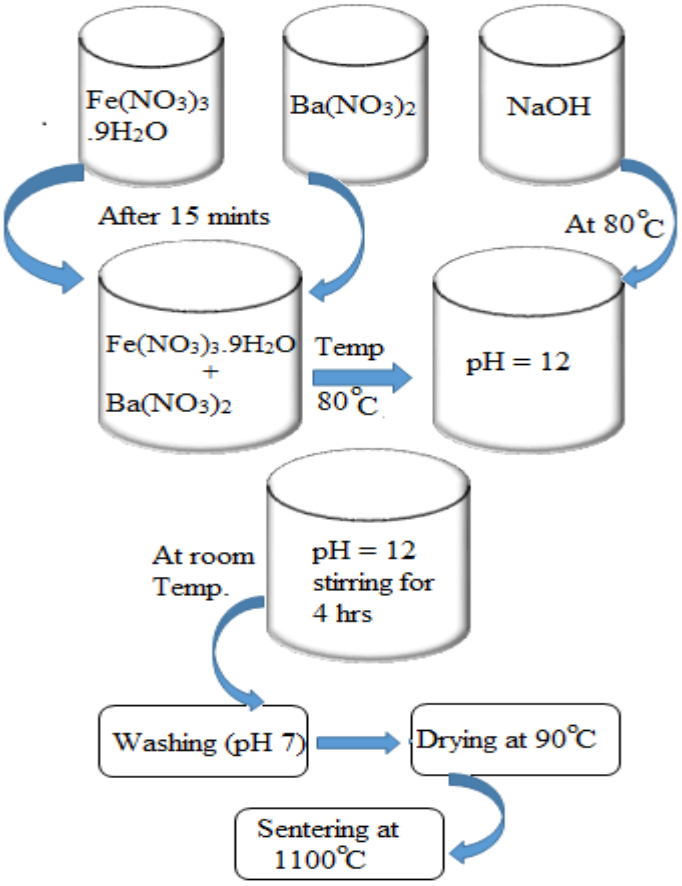

Fig 2.1. Schematic of Coprecipetation method.

2.3.1 Preperation of MWCNTs/$BaFe_{12}O_{19}$ composite

For the preparation of MWCNTs/$BaFe_{12}O_{19}$ composite "O-xylene" was used as a dispersing medium. In this process O-xylene was taken in four beakers of 100 ml and 2g of $BaFe_{12}O_{19}$ nanoparticles were added to them. Then the solutions were kept

in ultrasonicators for 6 hours. After obtaining homogeneous dispersion of O-xylene and ferrite nanoparticles, MWCNTs were added to the dispersions in calculated amount to get four samples S_1, S_2, S_3 and S_4 containing 1%, 2%, 3% and 5% by weight composition of MWCNTs/$BaFe_{12}O_{19}$ respectively. Then the dispersions were again ultrasonicated in the ultrasonicator for another 6 hours. When a homogenous dispersions were obtained, the dispersions were kept at room temperature to settle down and then kept in oven at 90^oC for overnight. After heating it for overnight the O-xylene evaporated from the composite leaving behing only MWCNTs/$BaFe_{12}O_{19}$ nanocomposites in solid form. Then the nanocomposites were crushed in powder form with the help of motar and pestle. The fine powder of composite were again sentered in muffle furnace at 400^oC for 4 hours.

(Chapter 3)

Experimental Techniques

3.1 Scanning Electron Microscopy (SEM)

The study of morphology (texture) and microstructure of a material is performed by the help of scanning electron microscopy (SEM). In this technique, the material or sample is irradiated by high-energy electron beam, which strike back from the surface of the sample. A variety of signals is generated from the surface of the sample according to its morphology or texture and is collected by a detector. A computer draws a 2-diamensional image from the information collected from the reflected electron beam, which displays the spatial variations in the properties of the sample. The following information can be obtained about the sample from scanning electron microscopy.

- Chemical composition Analysis
- Morphology or texture
- Crystalline structure & orientation of materials making up the sample

A conventional SEM technique can scan 1cm to 5 microns in width and can be imaged with magnification ranging from 20X to about 30000X and resolution ranging from 50 to 100 nm. A selected point location study of the sample can also be performed by SEM which is helpful in qualitatively or semi-qualitatively determining chemical composition by using EDS, crystalline structure, and crystal orientations by using EBSD. Different components of SEMs are shown in the following figure.

3.1.1 Working Principle

The incident electron beam consists of electrons having considerable amounts of kinetic energy. This kinetic energy is used the interaction of electron beam with the sample and produces a variety of signals. The signals obtained from the electron beam and sample interaction consist of Secondary electrons, back scattered electrons, Diffracted backscattered electrons, Photons produced from characteristic X-rays,

Visible light called cathode luminescence and Heat. Different components of SEM are shown in figure 3.1.

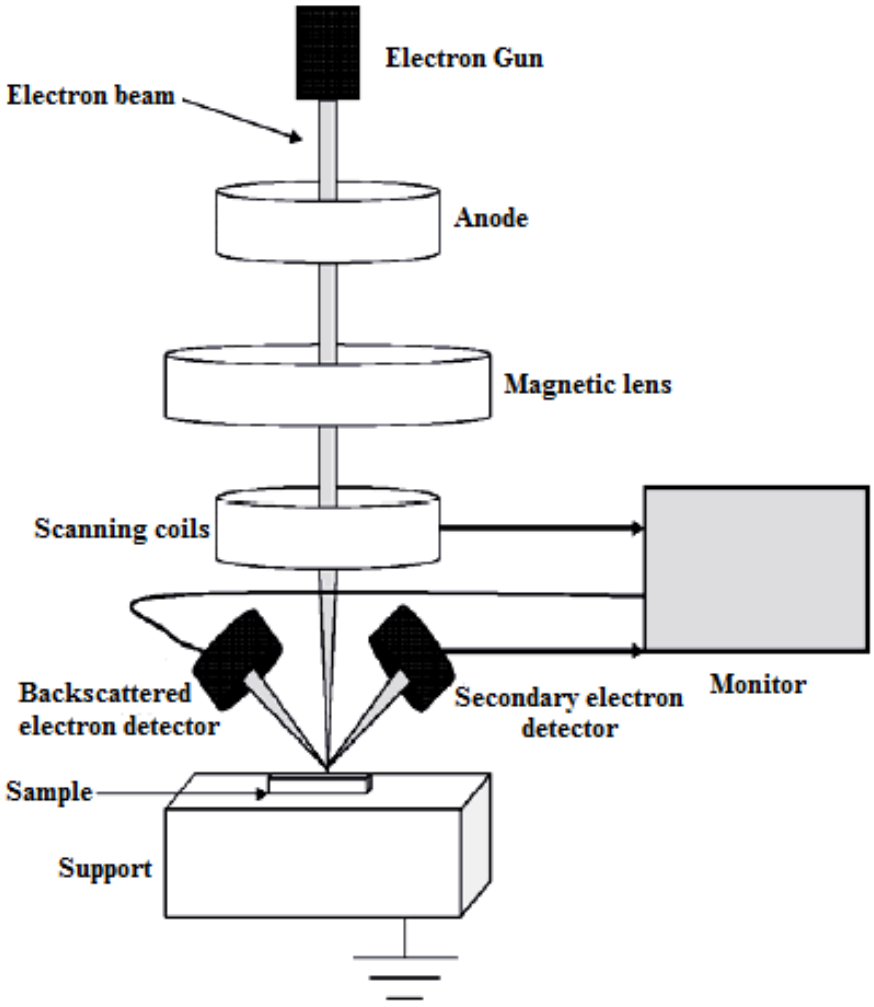

Fig. 3.1 Schematic diagram of scanning electron microscopy (SEM) [53]

The samples images are drawn from the information of secondary electron and back scattered electrons. The morphology of the sample is usually shown from the information of secondary electrons while the back scattered electrons are used in showing the contrasts of multiphase samples [54]. When the incident electrons interact with the discrete orbital's electrons of the sample and excite them to the upper levels then after their deexcitation, they emit X-rays that are of a fixed wavelength depending on the nature of the sample. SEM cannot change the nature or any other properties during its analysis, thus we can use a single sample repeatedly in SEM [55].

The spatial variation in chemical composition and high-resolution images are obtained from SEM technique. With the help of EDS, one can obtain elemental maps or spot chemical analyses. Back scattered electrons are used for the phase discrimination. The rapid discrimination of phases in multiphase samples are performed with the help of back scattered electron images. Diffracted backscattered electrons are very useful in the micro fabric and crystallographic orientation of different materials [55].

3.2 IR Spectroscopy

The presence and identification of chemical bond in a sample is found by using "Infrared Spectroscopy". In IR spectroscopy, the sample is irradiated with a full range of infrared frequencies. The infrared frequencies are absorbed by those molecules which vibrate with the similar frequencies. By absorption of infrared frequencies, the molecules get excited and in a short time they again deexcite to find stability which occurs in less than 10^{-6} seconds [8]. The energy released by molecules may be in the form of kinetic energy or in the form of photons. This absorption of frequencies of infrared light is measured by the spectrometer as a function of wavelength of light behind a sample. A transmittance or absorbance spectrum is plotted from the lack of intensities found at the molecule's vibrational frequencies and the chemical bonds present in the sample are determined through this way.

3.2.1 Fourier Transformation Infrared Spectroscopy

Fourier transformation infrared spectroscopy (FTIR) is a similar technique to IR spectroscopy. In FTIR an interferometer is used which split the IR radiation two beams having different optical distances which creates "alternating interferences fringes".

One of the most common interferometer is "Michelson interferometer". A Michelson interferometer consists of the following main arms [8].

- Infrared radiation source arm
- Stationary mirror arm
- Moving mirror arm
- Open arm

At the intersection of these four arms a beam splitter is placed which split the IR beam into two beams. Half of the IR beam pass through the beam splitter and falls on the fixed mirror where the remaining half strikes on the moving mirror. These two beams reflect back from the fixed and moving mirror respectively and combine again and then strike on the sample and then detected by the detectors [8].

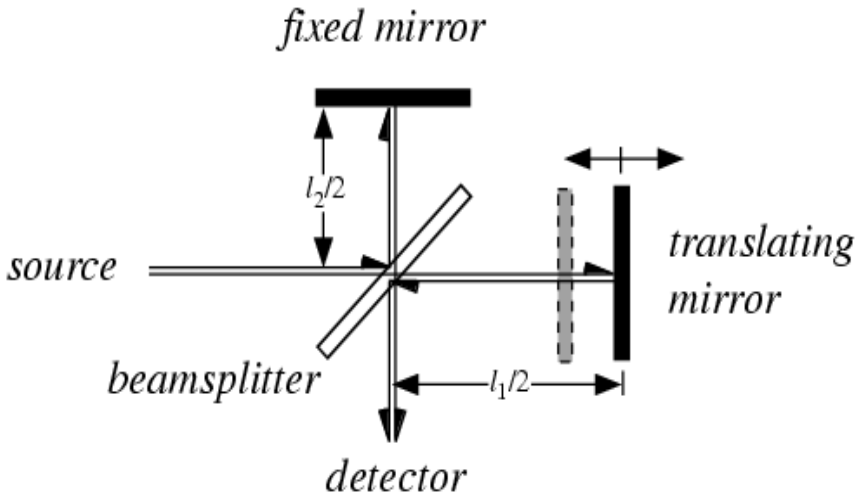

Fig 3.2. Michelson's interferometer [56].

The two beams reflected back from their respective mirror form a constructive interference pattern or destructive interference pattern depending on the length of the path provided by the moving mirror. FTIR spectroscopy become very useful technique as compare to convectional spectrometer, because it is a very economical, very sensitive and provide complete information about the sample in whole range of frequency in a very short time [57].

3.2.2 Uses of FTIR spectroscopy

FTIR is a widely used technique. Following are some characteristic features of FTIR spectroscopy.

- A small instrument and can carry easily from one place to other
- Give accurate measurements with the help of computer filters and results manipulation
- Can store a wide range of reference spectrums with which one can easily compare spectrum obtained from his sample.
- Can be used both for organic and inorganic materials

- Useful in verification and identification of sample
- Useful in the study of semiconducting materials
- Useful in measuring the degree of polymerization in polymers.
- Helpful in finding variation in quality of specific bonds

3.3 X-ray Diffraction (XRD)

Powder X-ray diffraction pattern is used for the crystallographic study of the sample. XRD pattern of a sample contains all information about the crystal structure of that substance. Thus, one can simply identify or characterize a polycrystalline substance through XRD technique. The crystal structure is identified by matching the peaks obtained in the XRD pattern with a reference or standard pattern of the same substance. After matching with the standard pattern, the crystallite size of the sample can also be calculated from the XRD pattern obtained for the sample [58].

In XRD technique the interaction of X-rays with the sample is studied. The sample is illuminated under X-rays, which interact with the crystal structure of the sample and then detected by a detector. Then a pattern is drawn according to the information which is obtained from the interacted light by the detector. The interaction between the X-rays and the crystal structure of the sample is governed by the Bragg's law, which is given mathematically as,

$$n\lambda = 2\mathrm{d}_{hkl} \sin\theta$$

In Braggs equation 'd' represent the inter-planner spacing and h,k,l and the planes, λ is the distance between two consecutive peaks (wavelength) of the X-rays used and 'θ' is the known as Bragg angle.

In XRD technique the sample is illuminated with X-rays, these X-rays interact with the and reflected back from the crystallographic planes of the sample. The X-rays reflected from the different crystallographic planes have some path difference. The path difference between a pair of reflected rays which are reflected from the two neighboring crystallographic planes are equal to the distance between two planes or inter-planner spacing. Thus, according to this the total path difference for a sample depends upon 'nλ' which is the product of integer (n) and wavelength (λ). These reflected rays cause interference and show constructive interference in the result of

that constructive interference X-ray pattern are drawn. The following figure show the interaction between the X-rays and the crystallographic planes of the sample.

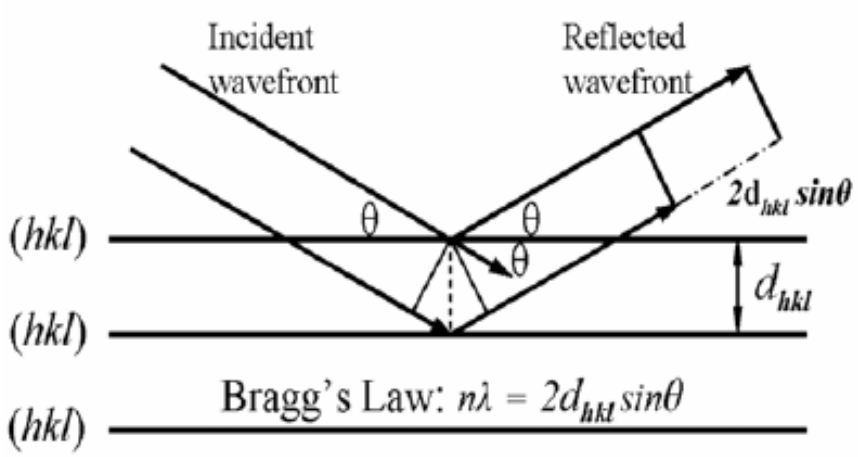

Fig 3.3. Crystal planes and Bragg's law [59]

In an X-ray diffractometer the first thing needed is the source of X-rays, most commonly use X-ray source is Cu from which the required X-rays are obtained for the XRD technique. The X-rays used in this technique should be of same wavelength i.e. monochromatic. To obtain the monochromatic X-rays, the rays are first passed through a Ni filter which acts as monochromatic, it absorbs the other wavelengths and let pass through a specific wavelength. When the monochromatic X-rays falls on the sample after interaction with the sample the beam is diffracted in every possible direction of 2θ. Then there is a detected which detects the diffracted beam. The detected actually detects the intensity of diffracted rays, and draw pattern according to the intensities. Then the computer software shows these diffracted patterns which plots the position and intensities of the diffracted peaks.

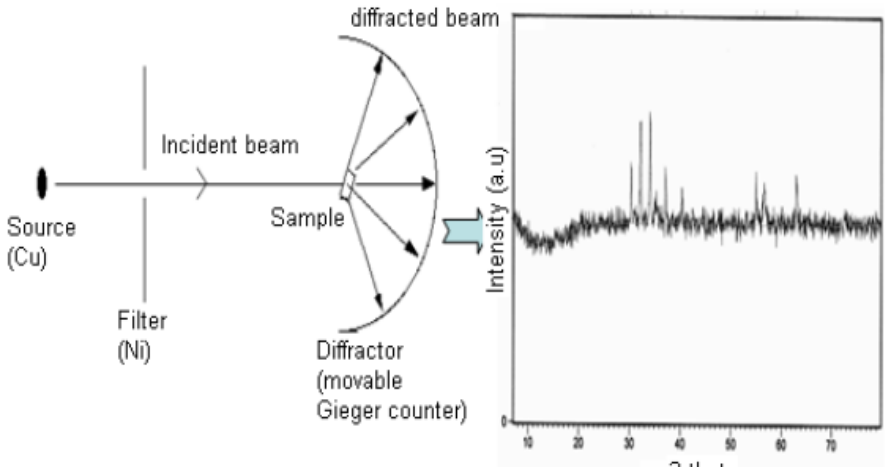

Fig 3.4. X-ray diffractometer [53].

The MWCNTs/$BaFe_{12}O_{19}$ nanocomposites in powder form annealed at 1100^{o}C were used in X-ray diffractometer. The peaks obtained in the XRD for all the synthesized samples were matched with the JCPD standard patterns found in the database, which indicated the hexagonal phase of the prepared samples. From that data, various parameters like X-ray density, cell volume crystallite size and lattice constant. The mathematical equations used for the calculation of the above discussed parameters were given below.

Scherrer equation can be used to calculate the size of nanomaterials studied in X-ray diffractometer. Scherrer equation is given as,

$$D = \frac{K\lambda}{\beta \cos\theta}$$

The variables used in Scherrer equation are:

λ – Wavelength of X-rays used (equal to 1.542 Å

K – constant (equal to 0.89 for hexagonal system)

β – Finite size broadening

To calculate the lattice constant (a & c) the following equation can be used.

$$\frac{1}{d^2} = \frac{4}{3}\left[\left(\frac{h^2 + hk + k^2}{a^2}\right) + \frac{l^2}{c^2}\right]$$

For the calculation of cell volume, the following equation can be used.

$$V_{cell} = 0.866\, a^2 c$$

The following equation were also used for calculating X-ray density and bulk density.

$$d_x = \frac{ZM}{N_A V_{cell}}$$

$$d_b = \frac{m}{\pi r^2 h}$$

Z – number of formula unit in a unit cell (2 for M-type hexaferrites)

M – molecular mass of the sample

N_A – Avogadro's number

m – mass of the pellet

h – height of the pellet

r – radius of the pellet

3.4 Dielectric Properties

The various factors affect the dielectric properties of ferrites, the most common in these factors are method of preparation, sintering temperature, grain size and relative concentration etc. The purpose of our thesis is to study the variation in the dielectric properties of MWCNTs/$BaFe_{12}O_{19}$ with increase in the MWCNTs from 0% to 5% by weight. The remaining factors which affect the dielectric properties of a composite are kept same for all same except the percentage of MWCNTs. The dielectric properties are studied at room temperature with the help of LCR meter bridge.

3.4.1 Dielectric Measurements

The pellets of MWCNTs/$BaFe_{12}O_{19}$ were prepared, the thickness of all the pellets was kept constant by applying same amount of pressure on them. The prepared pellets are of different composition containing (0,1,2,3 and 5%) MWCNTs. These pellets were fitted one by one in copper electrode to measure their capacitance. The dielectric constants were measured for each sample by using the following equation.

$$\varepsilon = \frac{C \times D}{A\varepsilon_o}$$

In above equation 'ε_o' is the permittivity of free space and ε is the permittivity of the material and known as the dielectric constant of that material because dielectric constant is the quantitative measure of the degree to which the material resists the flow of charges. In other variables C is the capacitance of the material and D is the thickness of the pellet where A is the area of the pellet. The capacitance was measured for each sample in the frequency range between 100Hz – 5 MHz at room temperature.

3.4.2 Dielectric loss

There are two types of losses in all material mediums the first one is known as conduction loss and the other one is dielectric loss. The conduction loss is related to the actual flow of charges through the dielectric. Where the former one i.e. dielectric loss is related to the movement or rotation of the atoms and molecules in a dielectric material present in an alternating electric field. The dielectric loss for the prepared samples was also calculated individually, the equation used for the calculation of dielectric loss was given as

$$\varepsilon' = \varepsilon \times D - factor$$

The D-factor was also calculated by the LCR meter with the capacitance.

3.4.3 Loss Tangent

The loss tangent is the parameter which is related to the energy dissipation of the material. Any material which stores energy dissipate that energy with time, some dissipate it very quickly some takes long time for dissipation; thus the loss tangent is that parameter which compute this dissipation of a material. For a good conductor or a good capacitor, the loss tangent should be small because if it is greater for a material then the most part of the energy will be dissipated inside the material in the form of heat or radio frequencies in air.

The loss tangent is calculated with the help of following equation.

$$Tan\ \delta = \frac{\varepsilon'}{\varepsilon}$$

The material which has high dielectric constant, low dissipation factor or Tan loss and high breaking voltage, low cost and can be easily fabricated will be

ideal dielectric material. It is impossible till known to obtain such a material which has perfectly controlled all parameters, but different materials with different controlled parameters individually were obtained and these materials are using in different fields for different purposes. In present case, we studied MWCNTs/$BaFe_{12}O_{19}$ nanocomposite, we find their different properties and discussed them.

3.4.4: Impedance

Impedance of a material is the resistance offered by the material to the flow of electron across its. As the electron hope between different ion sites like Fe^{2+} and Fe^{3+} ions sites in most of the ferrites. The behavior of impedance for a material can be characterized with the help of LCR meter. The real and imaginary parts of impedance can be calculated with the help of following equations.

$$\text{Real part of } Z = Z\cos(\varphi)$$

$$\text{Imaginary part of } Z = Z\sin(\varphi)$$

Where "φ" is phase angle which is given as

$$\varphi = tan - 1\left(\frac{X}{R}\right)$$

Where "X" is the reactance and R is the resistance obtained with the help of LCR meter.

3.4.5: Electric Modulus

Electric modulus is a very useful phenomenon which can be used to characterize the conduction and relaxation behavior of ionic and conducting ceramic materials. The complex electric modulus is also defined as the inverse of complex relative permittivity. The real and imaginary part of electric modulus was calculated by the help of following equations.

$$Real\ Part: M' = \frac{\varepsilon'}{(\varepsilon')^2 + (\varepsilon'')^2}$$

$$Imaginary\ Part: M'' = \frac{\varepsilon''}{(\varepsilon')^2 + (\varepsilon'')^2}$$

(Chapter 4)

Results and Discussion

4.1 X-Ray Diffraction

The structure of $BaFe_{12}O_{19}$ nanoparticles and its composite with MWCNTs was study with the help of X-ray diffraction technique. This structure analysis was done by CuKα radiations of 1.5418Å and scanning angle 2θ where θ ranging from 20 – 80 degrees. Fig 4.1 shows the XRD pattern for $BaFe_{12}O_{19}$ nanoparticles. The peaks were indexed from JCPDS (Joint Committee on Powder Diffraction Standards) card (JCPDS 00-043-0002), standard for $BaFe_{12}O_{19}$ nanoparticles. The XRD pattern of $BaFe_{12}O_{19}$ confirmed the desired hexagonal phase of $BaFe_{12}O_{19}$ was obtained along with some phases of Fe_2O_3. The phases for Fe_2O_3 were formed due to some incomplete reactions in the material. These peaks can be eliminated at higher annealing temperature. Scherer's formula was used to calculate the average crystallite size. The average crystallite size was 35 ± 5 nm.

Fig 4.2 shows the XRD patterns for all the prepared samples. All the peaks were matched with the JCPDS card (00-043-0002), the XRD peak for MWCNTs in the composites was not found due to presence of MWCNTs in very small amount in samples S_1 to S_4. The absence of characteristic peak (002) of MWCNTs in XRD graphs of S_1 to S4 indicated the complete anchoring of Barium nanoparticles on the outer surface of MWCNTs and also shows the minimum stacking of MWCNTs over each other. All the samples showed hexagonal phases and the peaks were matched with the JCPDS card (00-043-002). The crystallite size for all sample was determined by considering the intense peak (0 0 8), which is the characteristic peak of $BaFe_{12}O_{19}$ nanoparticles. The crystallite size was found in 35 ± 5 nm.

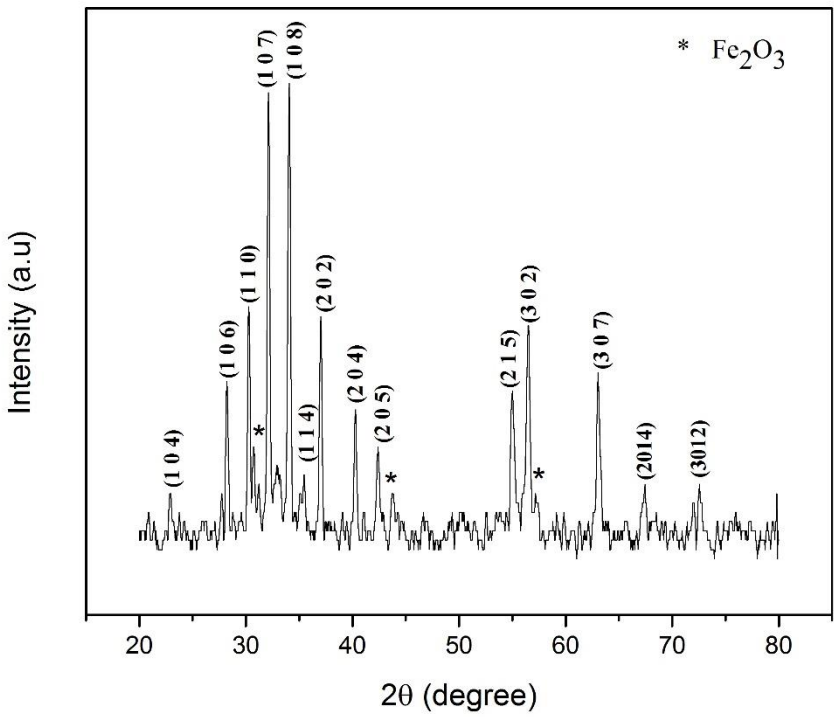

Fig 4.1. Indexed XRD pattern of $BaFe_{12}O_{19}$ nanoparticles.

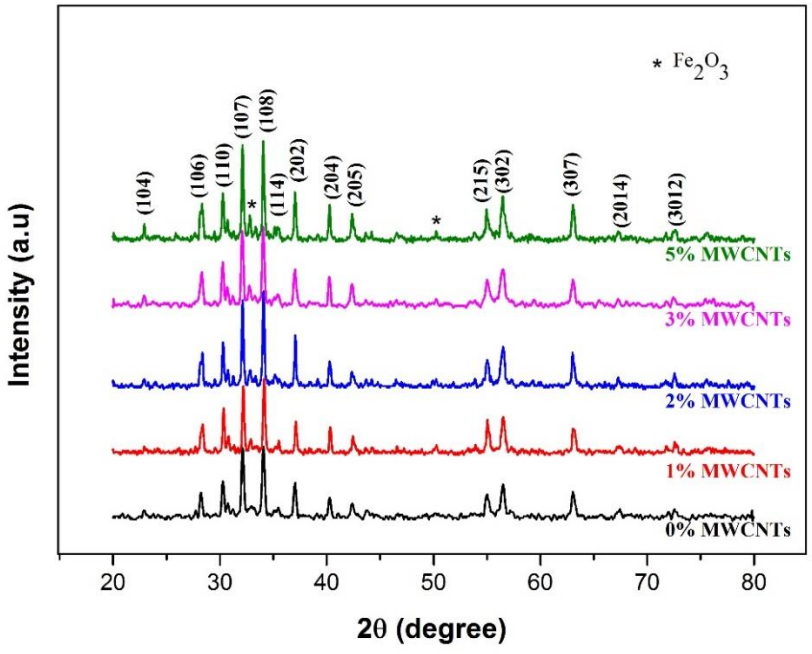

Fig 4.2 XRD pattern of $BaFe_{12}O_{19}$ and its prepared nanocomposites

4.2 Scanning Electron Microscopy SEM

The morphological study of $BaFe_{12}O_{19}$ nanoparticles prepared by co-precipitation method and $BaFe_{12}O_{19}$/MWCNTs nanocomposite prepared by ultra-sonication method was carried out by low vacuum scanning electron microscope (JSM-6490A), operated at 20 KV with magnification range 100X ~ 70000X. The samples were dispersed in double distilled water with the help of ultra-sonication and when uniform dispersions were obtained then drops of dispersions were dropped on a glass slide and then dried. The samples were gold coated of 25Å with the help of Sputter Coater (JFC1500) to made them conductive. Fig 4.3 showing the SEM image of $BaFe_{12}O_{19}$ nanoparticles synthesized by co-precipitation method at 1100^{o}C. The nanoparticles were well dispersed and showed no agglomeration. The average particles size obtained was 25.7 ± 5 nm. Fig 4.4 showing the SEM image of MWCNTs. The average diameter obtained for MWCNTs was 38.9 ± 6 nm. Fig 4.5 showing the SEM image of $BaFe_{12}O_{19}$/MWCNTs nanocomposite prepared by ultra-sonication method. From the image it is clear that the nanoparticles are attached at the surface of MWCNTs.

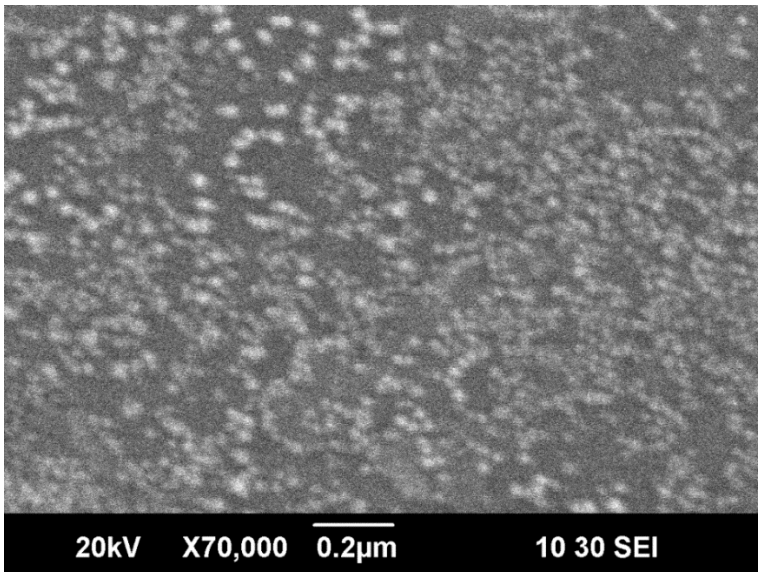

Fig. 4.3 SEM image of $BaFe_{12}O_{19}$ nanoparticles.

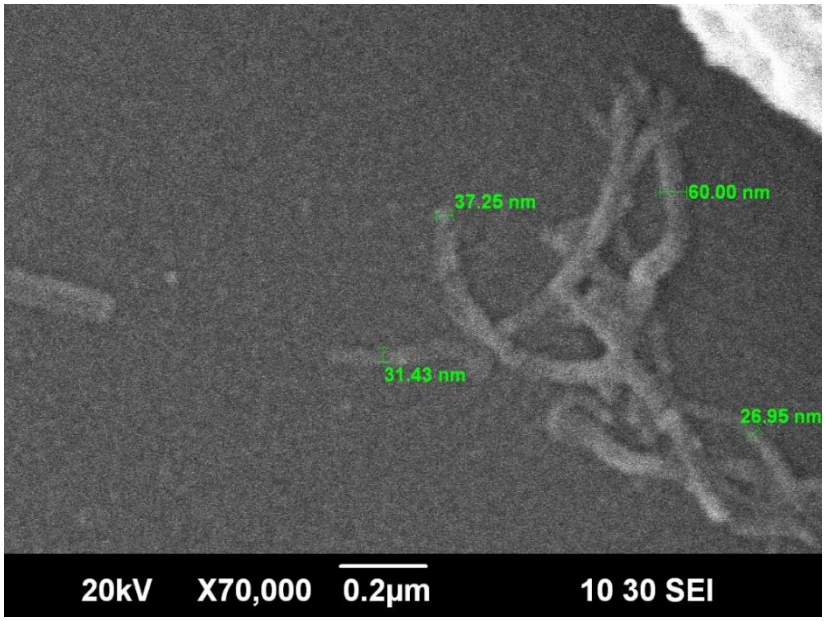

Fig.4.4 SEM image of MWCNTs

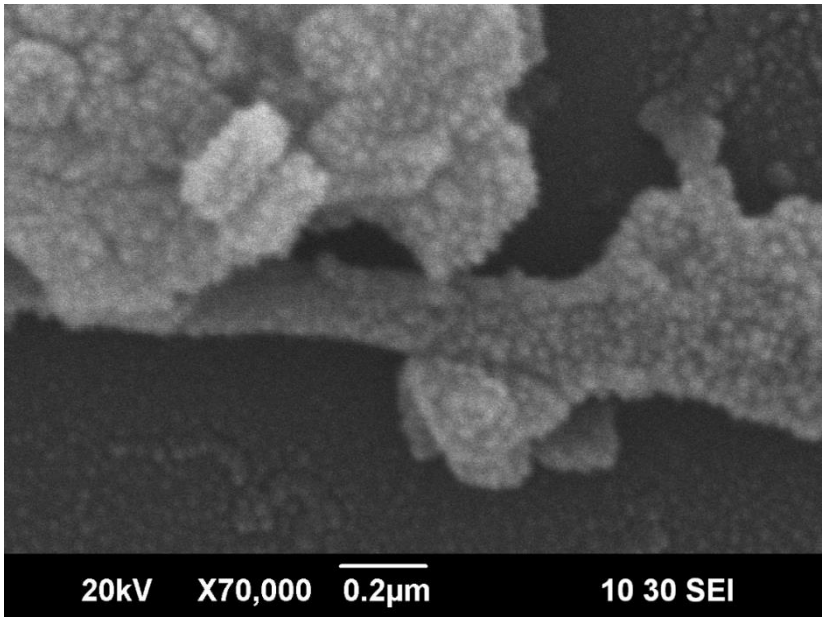

Fig 4.5. SEM image of $BaFe_{12}O_{19}$/MWCNTs nanocomposite.

4.3. Fourier Transform Infrared Spectroscopy (FTIR)

Fourier transform infrared spectroscopy (FTIR) was done by illuminating the samples with infrared waves of wavelength (350-4000 cm^{-1}). The FTIR was carried out with the help of (Perkin Elmer-spectrum 100) FTIR spectroscope using KBr pallets. Fig 4.6 shows the absorption spectra of FTIR for $BaFe_{12}O_{19}$ nanoparticles and $BaFe_{12}O_{19}$/MWCNTs nanocomposite. In case of simple $BaFe_{12}O_{19}$ nanoparticles the absorption peaks were obtained at 434.47,598.43 and 1431.80 cm^{-1}. The stretching bands at 434.47 and 598.43 are associated with the M-O bands at octahedral ion sites and tetrahedral ion sites. The absorption peaks occur around 580 ~600 cm^{-1} are due to the metal-oxygen bands at octahedral sites where the absorption peaks that occur around 400 cm^{-1} are due to metal-oxygen bands stretching vibration at tetrahedral sites.[60]

When a composite of $BaFe_{12}O_{19}$ and MWCNTs was prepared containing only 1% of MWCNTs then the absorption peaks found in the case of pristine $BaFe_{12}O_{19}$. In this case the above mentioned vibrational bands are shifted to 437.04 cm^{-1} and 608.95 cm^{-1} from 434.47 cm^{-1} and 598.43 cm^{-1} respectively. In case of $BaFe_{12}O_{19}$/MWCNTs nanocomposite containing 2% MWCNTs these vibrational bands are shifted to 442.12 cm^{-1} and 607.09 cm^{-1} from 434.47 cm^{-1} and 598.43 cm^{-1} respectively. Similarly, in case of $BaFe_{12}O_{19}$/MWCNTs nanocomposite containing 3% MWCNTs these vibrational band are shifted to 439.10 cm^{-1} and 607.15 cm^{-1} and in case $BaFe_{12}O_{19}$/MWCNTs nanocomposite containing 5% MWCNTs these absorption peaks were found at positions 437.04 cm^{-1} and 608.95 cm^{-1}.

The shift in vibrational bands of $BaFe_{12}O_{19}$ occurs due to the attachment of $BaFe_{12}O_{19}$ nanoparticles on the walls of MWCNTs and this give an evidence about the successfully attachment of nanoparticles on the outer walls of MWCNTs. Similar behavior was found by Nahid Shiri et al[61]. The stretching bands at 1431.80 cm^{-1}, 1437.69 cm^{-1}, 1441.96 cm^{-1}, 1425.82 cm^{-1} and 1437.69 in case of $BaFe_{12}O_{19}$ and nanocomposite containing 1,2,3 and 5% MWCNTs respectively are associated with the water which was in KBr used for the formation of pallets. Moreover, the FTIR spectra of MWCNTs used in this research appeared at 3393, 3429 and 3429 in case of the samples containing 2%, 3% and 5% MWCNTs. The characteristic peak of

MWCNTs in case of nanocomposite containing only 1% MWCNTs is not visible due to very small amount of MWCNTs in the mentioned sample.

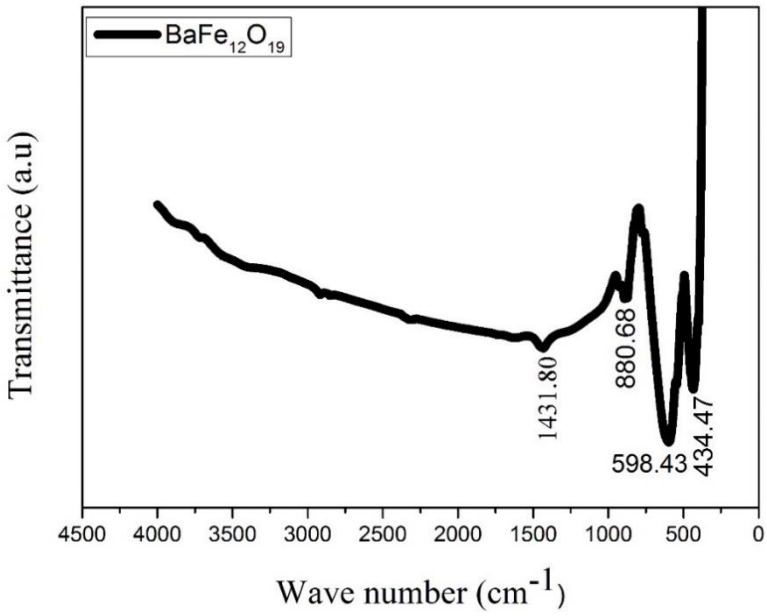

Fig. 4.6(a) FTIR spectra of $BaFe_{12}O_{19}$

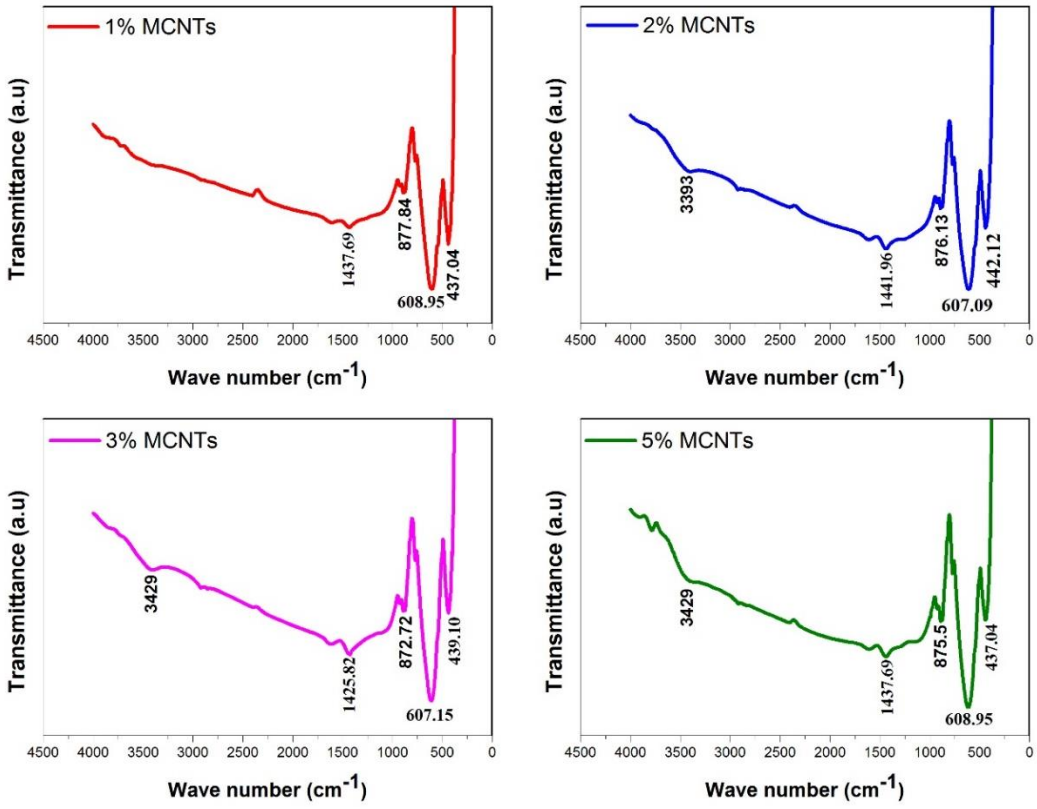

Fig. 4.6(b) FTIR spectra of prepared $BaFe_{12}O_{19}$/MWCNTs containing 1% ,2% 3% and 5% MWCNTs respectively.

4.4. Dielectric Properties

The dielectric properties of $BaFe_{12}O_{19}$/MWCNTs nanocomposite was measured with the help of LCR meter (WK-6500B) in the range of 1MHz – 1GHz frequency. From LCR meter we obtained change in Dielectric constant, Dielectric loss (real permittivity), Tan loss (imaginary permittivity) and A.C conductivity relative to frequency. The plot between frequency and Dielectric constant is given in fig 4.7. It is an theoretical assumption that the dielectric constant decreases as the frequency increases [62]. As the dielectric constant is due to polarization of material and in ferrites the polarization occurs due to transfer of electrons between Fe^{2+} and Fe^{3+} sites. As the frequency increases it decrease the transfer rate of electrons between Fe^{2+} and Fe^{3+} ions, and after a certain frequency limit this exchange of electrons stops and do not follow the alternating field, thus after that certain limit or frequency the dielectric remains constant [63].

In case of sample of $BaFe_{12}O_{19}$ with 0% MWCNTs, the LCR-meter measured the dielectric constant as 7.7×10^5 at lower frequency and it decreases with increase in frequency as per theoretical assumptions and after a certain frequency it became constant. As it is shown in the plot that the dielectric constant is increased at lower frequencies as we increase the wt% of MWCNT in $BaFe_{12}O_{19}$/MWCNTs nanocomposite. Due to increase in wt% of MWCNTs the rate of exchange of electrons between Fe^{2+} and Fe^{3+} is enhanced which in result enhance the polarization. The dielectric constant measured at lower frequency (100Hz) for $BaFe_{12}O_{19}$/MWCNTs nanocomposite containing 1% MWCNTs and 99% $BaFe_{12}O_{19}$ has the 1.31×10^6. Similarly, for 2, 3, and 5% MWCNTs it is 1.47×10^6, 1.8×10^6 and 2.48×10^6 respectively.

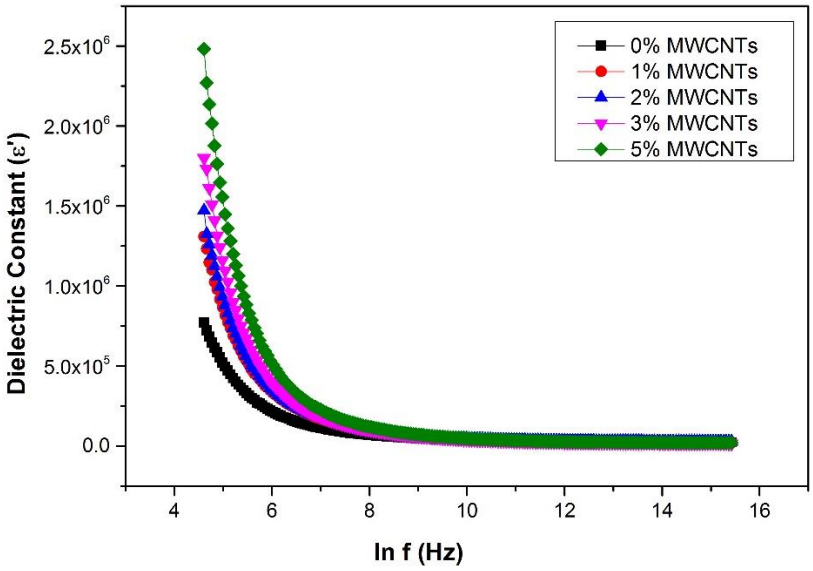

Fig 4.7 Graph between Frequency and Dielectric constant

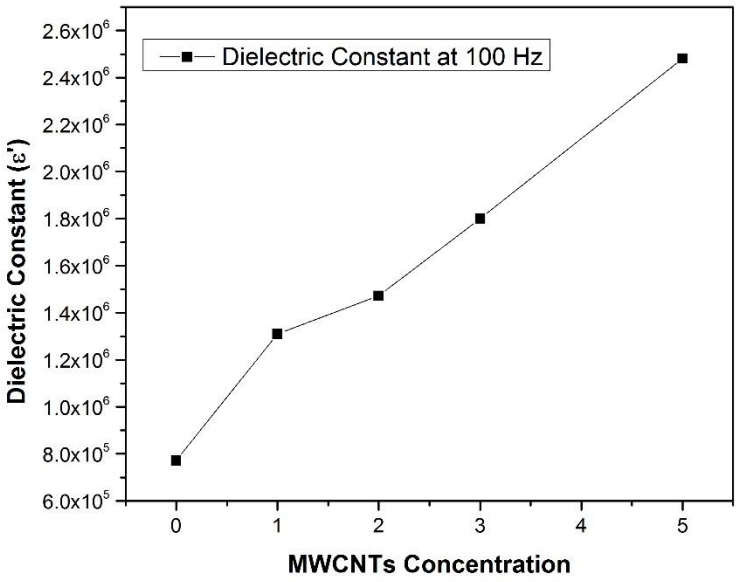

Fig 4.8 Dielectric constant values at 100 Hz.

Sample	Dielectric constant	Dielectric Loss	Tan loss
0% MWCNTs	7.7×10^5	1.54×10^6	2.00
1% MWCNTs	1.3×10^6	3.07×10^6	2.34
2% MWCNTs	1.47×10^6	3.60×10^6	2.45
3% MWCNTs	1.80×10^6	5.10×10^6	2.83
5% MWCNTs	2.48×10^6	7.69×10^6	3.1

Table 4.1. Values of mentioned properties at initial frequency.

Fig 4.9 shows the graph between frequency and dielectric loss. The imaginary permittivity (dielectric loss) also decreases theoretically with increase in frequency and become constant after certain frequency. In the graph (4.9) similar trends was obtained from our samples. For $BaFe_{12}O_{19}$ sample containing 0% MWCNTs has

imaginary permittivity equal to 1.54×10^6 at lower frequency but it decreases with increase in frequency and then become constant.

As in case of $BaFe_{12}O_{19}$ with 0% MWCNTs the value of imaginary permittivity is equal to 1.54×10^6 and from the graph it is clear that value of imaginary permittivity increases as we increase the wt% of MWCNTs in $BaFe_{12}O_{19}$/MWCNTs nanocomposite samples. The values imaginary permittivity for 1,2,3 and 5% MWCNTs nanocomposite are 3.07×10^6, 3.60×10^6, 5.10×10^6 and 7.69×10^6 respectively. The values are given in Table 4.1. Fig 4.10 shows the values of dielectric loss at 100 Hz for each sample.

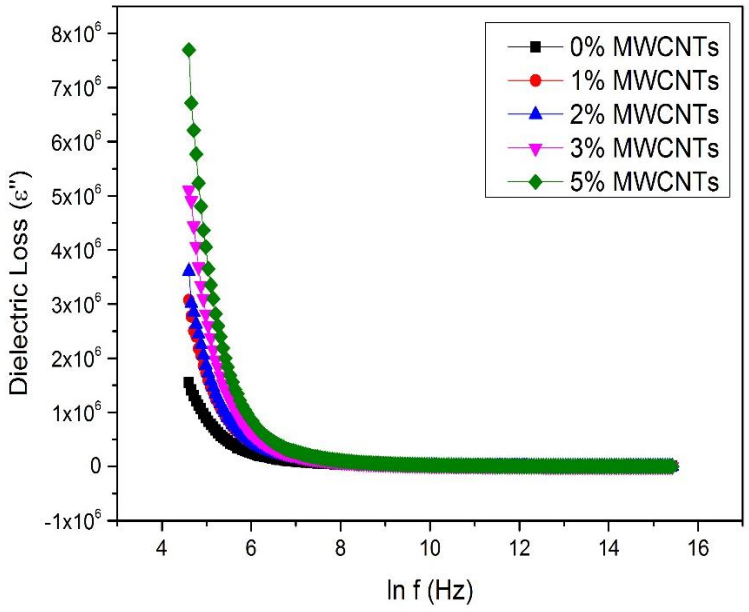

Fig. 4.9 Graph between Frequency and Dielectric loss (imaginary permittivity).

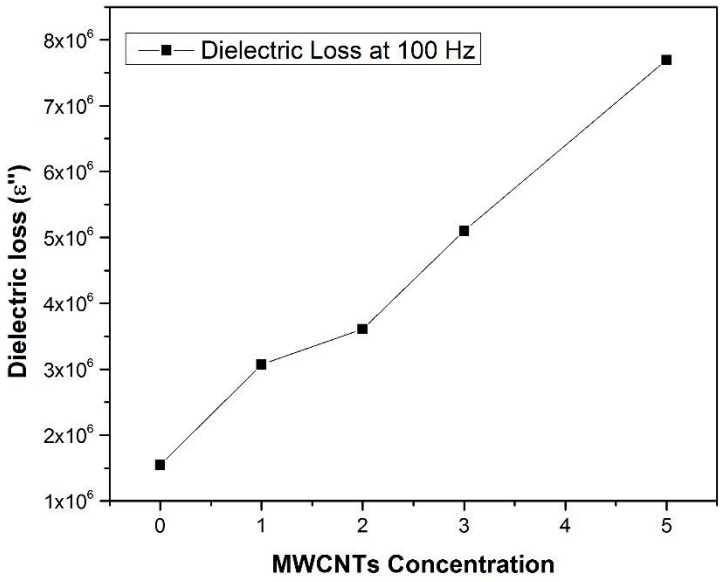

Fig 4.10 Dielectric loss values at 100 Hz

Fig 4.11 shows the relation between frequency and dielectric loss tangent (tan δ). Dielectric loss tangent also showed similar behavior as dielectric constant and dielectric loss. It also decreased with increase in frequency and become constant after a certain value of frequency. Tan loss also increased with increase in wt% of MWCNTs. The value of tan loss factor for each sample is given in Table 4.1. The values of dielectric loss tangent measured at 100 Hz is graphically represented in Fig 4.12 for each sample.

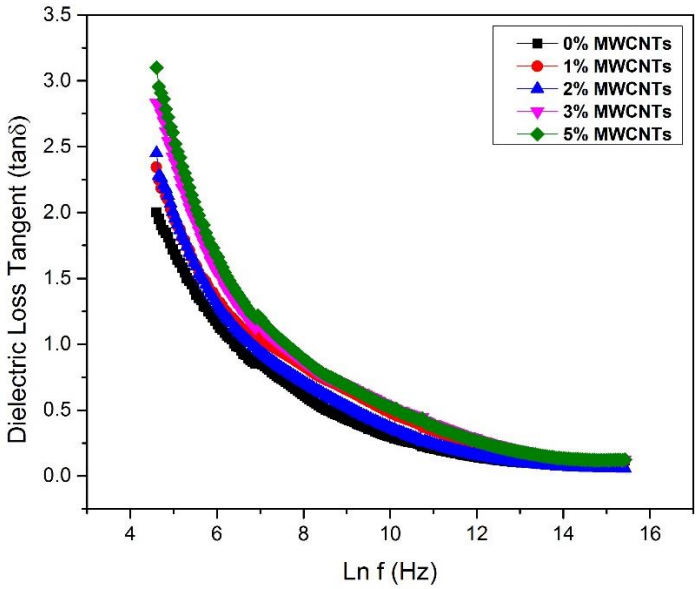

Fig 4.11 Graph between Frequency and Tan loss.

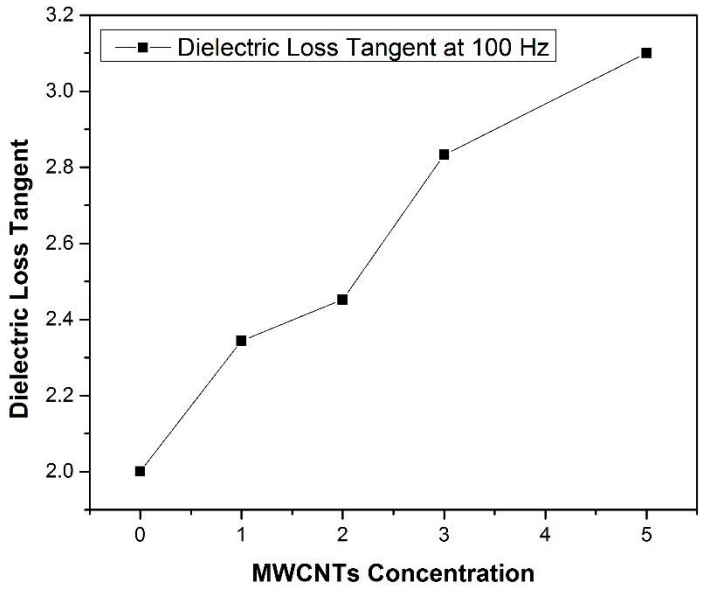

Fig 4.12 Dielectric loss tangent values at 100 Hz

Fig. 4.13 shows the variations of AC conductivity. AC conductivity in ferrites can be explained by hopping model[64]. The MWCNTs having conductive nature provide a specific path for the hopping of electrons between the ions of ferrites and due to which the AC conductivity also increases with increase in wt% of MWCNTs in $BaFe_{12}O_{19}$/MWCNTs nanocomposites. The AC conductivity for the sample

containing 0% MWCNTs is minimum at 100 Hz where it is maximum for the sample containing 5% MWCNTs at particular frequency. Increase in A.C conductivity with increase in frequency indicates the dominance of hoping conductivity over band conductivity. Similar trend was obtained for our samples which is shown in fig 4.13.

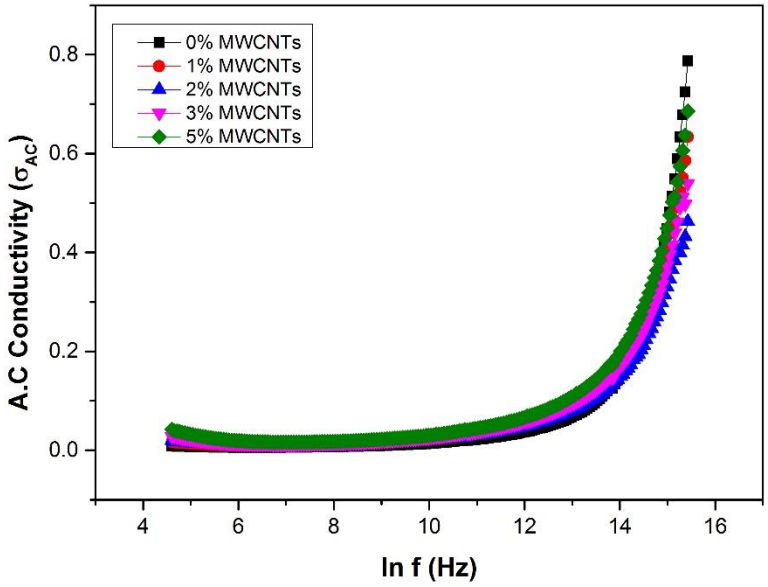

Fig 4.13 Graph between Frequency and AC conductivity

4.5 Impedance

Impedance was measured by the same LCR-meter used for finding the dielectric properties of our sample and in the same range of frequency. Fig 4.14 is the plot obtained from the data of LCR-meter, which is between the frequency applied and impedance measured. Like other electrical properties the impedance also showed similar trend which higher at lower frequency and then decreasing with increase in frequency and after that it become constant. Impedance is also affected with the flow of electrons between the Fe^{2+} and Fe^{3+} ions in ferrites. In Fig 4.14 the impedance decreases as we increase the wt% ratio of MWCNTS in $BaFe_{12}O_{19}$/MWCNTs nanocomposite. Fig 4.15 shows variation occurred in impedance at 100 Hz for each sample. The attachment of $BaFe_{12}O_{19}$ nanoparticles on the walls of MWCNTs provide a specific smooth way for the flow of electrons between the ions of ferrites which decrease the impedance or resistance offered to the flow of electrons. The impedance

value for $BaFe_{12}O_{19}$ was 1.3×10^8 which was decreased to 3.6×10^7 for $BaFe_{12}O_{19}$/MWCNTs containing 5% MWCNTs. The impedance values for each sample is given in Table 4.2. The graphs for the real and imaginary part of the impedance are shown in Fig 4.14 and 4.16 respectively drawn by using the following equations.

$$Real\ part\ of\ Z = Zcos(\varphi)$$

$$Imaginary\ part\ of\ Z = Zsin(\varphi)$$

Where "φ" is phase angle which is given as

$$\varphi = \tan^{-1}\frac{X}{R}$$

X is the reactance and R is the resistance obtained with the help of LCR meter.

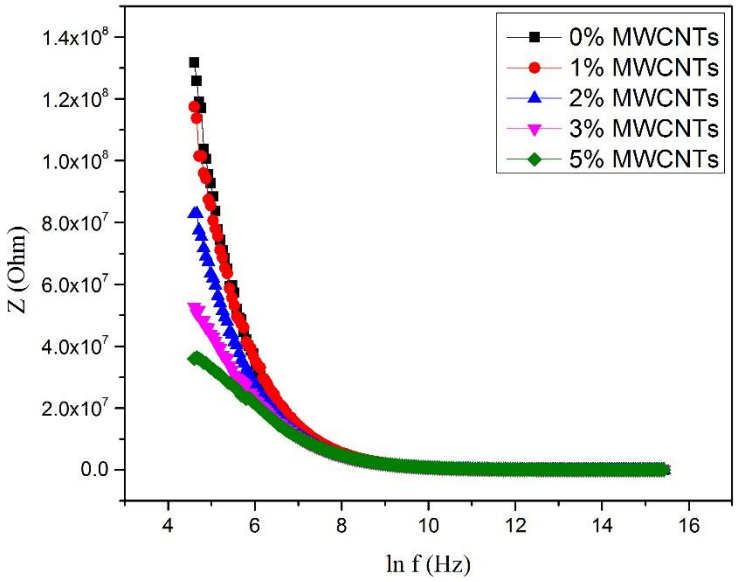

Fig 4.14 Graph between frequency and Impedance (real part of impedance)

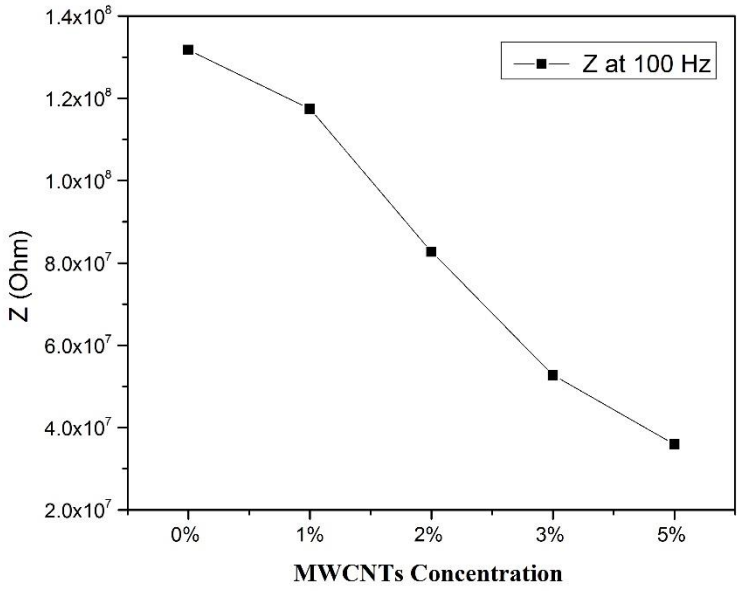

Fig 4.15 Values of impedance at 100 Hz (real part of impedance)

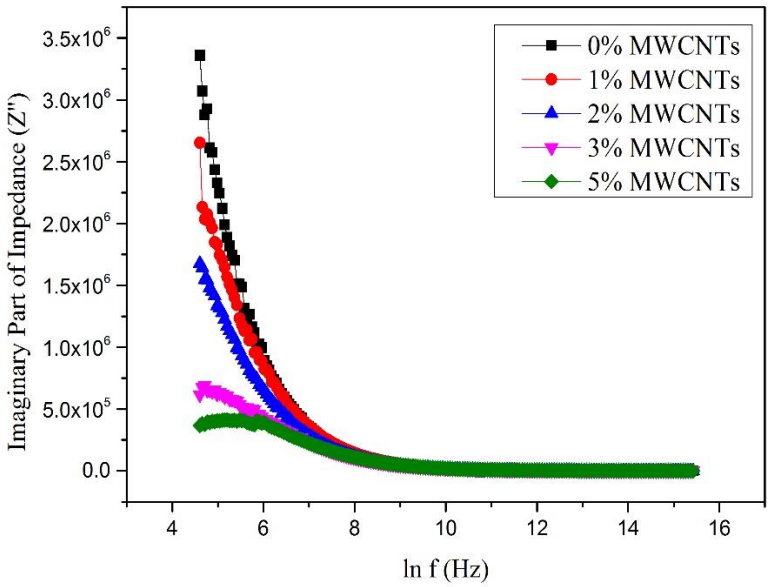

Fig 4.16 Graph between Frequency and Imaginary part of impedance (Z")

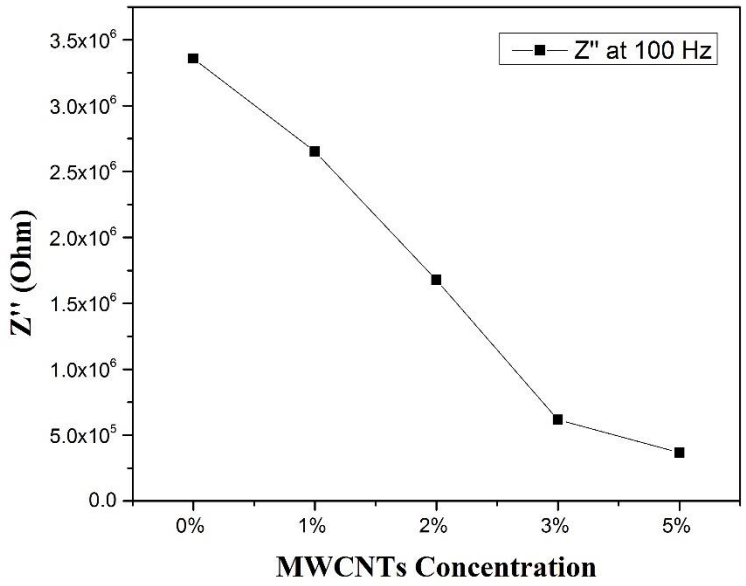

Fig 4.17 Values of imaginary part of impedance at 100Hz

Sample	Impedance	Real Part	Imaginary Part
0% MWCNTs	1.3×10^8	1.3×10^8	3.3×10^6
1% MWCNTs	1.1×10^8	1.2×10^8	2.6×10^6
2% MWCNTs	8.2×10^7	8.3×10^7	1.6×10^6
3% MWCNTs	5.2×10^7	5.3×10^7	6.2×10^5
5% MWCNTs	3.5×10^7	3.6×10^7	3.6×10^5

Table 4.2. Calculated values for Impedance and its Real and Imaginary part

4.6 Electric Modulus

Electric modulus is a very useful phenomenon which can be used to characterize the conduction and relaxation behavior of ionic and conducting ceramic materials. The complex electric modulus is also defined as the inverse of complex relative permittivity. Fig 4.18 and 4.19 shows the behavior of real and imaginary part of Electric modulus with respect to frequency. Where Fig 4.21 shows the graph between Real part of Electric modulus (M') and imaginary part of electric modulus (M'') which is also known as Cole-Cole diagram. The real and imaginary part of electric modulus was calculated by the help of following equations.

$$Real\ Part: \quad M' = \frac{\varepsilon'}{(\varepsilon')^2 + (\varepsilon'')^2}$$

$$Imaginary\ Part: \quad M'' = \frac{\varepsilon''}{(\varepsilon')^2 + (\varepsilon'')^2}$$

As we discussed that the electric modulus or complex electric modulus shows the conduction and relaxation behavior, in Fig 4.18 the real part of electric modulus decreases as we increase the wt% of MWCNTs in $BaFe_{12}O_{19}$/MWCNTs nanocomposite. The decrease in the electric modulus indicates the increase in the conductivity of our samples due to increase in the wt% of MWCNTs. Fig 4.19, shows the behavior of imaginary part of electric modulus with respect to frequency. In which, the dielectric response of our samples against variation in frequency is represented in the form semi-circle arcs. In the figure, the maximum values of arcs are shifted towards the higher frequency as we increase the wt% of MWCNTs in our nanocomposite. This change in the imaginary part of electric modulus shows the relaxation rate, the relaxation rate is decreases as the peaks are shifted towards the high frequency range. The values for imaginary part of electric modulus (M") in the start increases with increase in frequency i.e. the dipole oscillated frequency increases with applied frequency and then at a certain value where the oscillating frequency matches the applied frequency give us a maximum on the graph and known as relaxation frequency. After the relaxation frequency is achieved the graph is shifted toward the lower values of M" due to increase in grain boundaries contribution to resistance. Fig 4.21 shows the graph between real and imaginary part of Electric modulus i.e. M' vs M", this graph is also known as Cole-Cole diagram. It is obvious

from Fig 4.21 that the maximum of the arcs shifted toward the higher values of M' as we increase the content of MWCNTs in nanocomposite. This behavior shows that the relaxation rate is decreases and the conduction of the electrons increases which in result increases the conductance of our sample. Thus, the increase in the wt% of MWCNTs in the $BaFe_{12}O_{19}$/MWCNTs make the material more conductive which increase the dielectric loss.

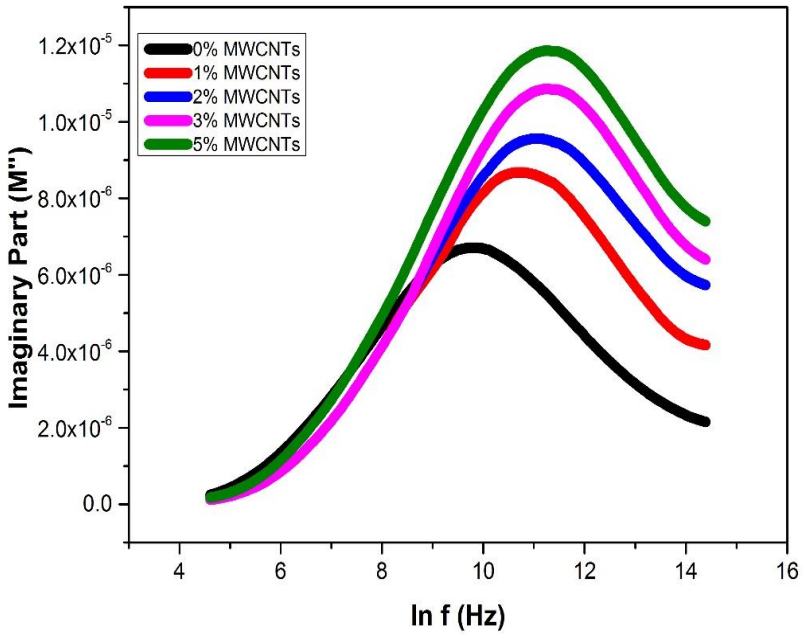

Fig 4.18 Graph between frequency and Imaginary part of Electric Modulus (M")

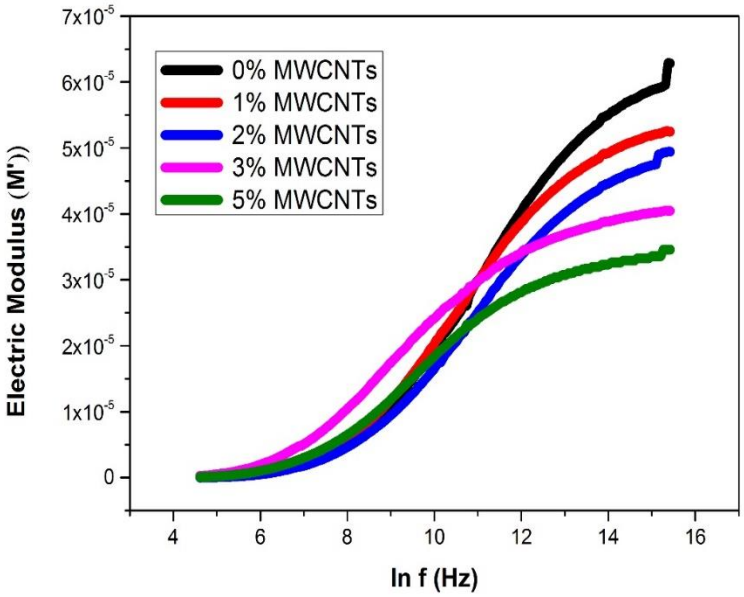

Fig 4.19 Graph between frequency and Real part of Electric Modulus (M')

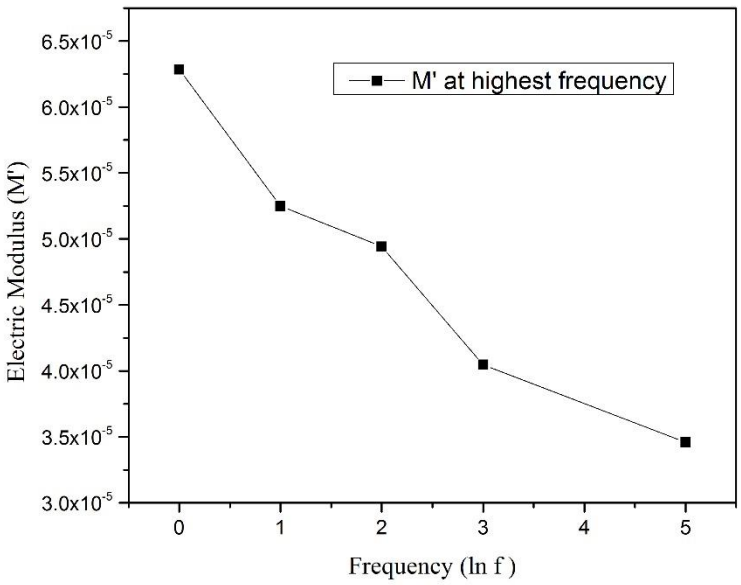

Fig 4.20 Values of Real part of Electric modulus (M') at highest frequency

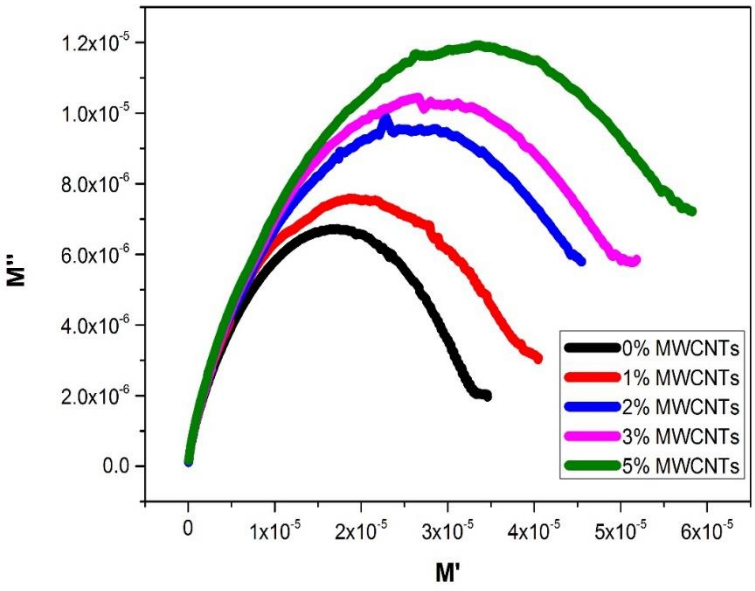

Fig 4.21 Cole-Cole plot. Graph between Real and Imaginary part of Electric Modulus

4.7 DC Electric Resistivity

DC resistivity is measured for $BaFe_{12}O_{19}$ and its composited with different concentration of MWCNTs as a function of temperature. The plots for the measured DC resistivity is shown in Fig 4.22. The plot representing $BaFe_{12}O_{19}$ shows a gradual decrease in the resistivity with increase in temperature. By increase in temperature the electrons get more energy which makes the conduction of electrons across the sample easier and hence its resistivity decreases at higher temperature. The DC resistivity decreased as we increased the wt% of MWCNTs in our $BaFe_{12}O_{19}$/MWCNTs. By increase in MWCNTs the Dc resistivity decreases due to the electrical properties and conductive nature of MWCNTs. The MWCNTs are providing easy paths for the conduction of electrons due to which the DC resistivity in decreased.

The DC resistivity was measured from temperature and current value at constant voltage.

As we know that

$$\rho = \frac{R \times A}{L}$$

Where 'R' is the calculated resistance by V = IR, 'A' is the area of sample used and 'L' is the length or thickness of our sample.

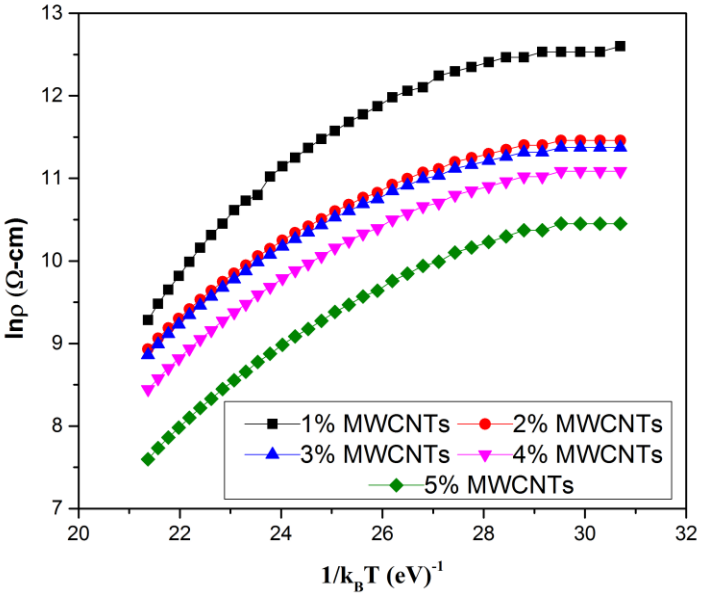

Fig 4.22 Composition variation of dc electrical resistivity (lnρ) with $1/k_BT(eV)^{-1}$

4.7.1 Drift Mobility

$$Drift\ Mobility = \mu_d = \frac{1}{ne\rho}$$

In the equation above,

e = charge on electron

ρ = Resistivity

and n = concentration of charge carriers

The following equation can be used to find charge carrier's concentration.

.

$$n = \frac{N\rho_m P_{Fe}}{M}$$

Where,

N = Avogadro's number

M = Molecular weight

ρ_m = Measured density

and P_{Fe} = No of iron atoms in the chemical formula of ferrite

For calculating measured density following formula was used

$$\rho_m = \frac{m}{\pi r^2 h}$$

By use of above mentioned equations we found the drift mobility of our samples and then draw it against "$1/k_BT$" as shown in Fig 4.23. In the graph, the drift mobility against "$1/k_BT$" is higher at lower values and then decreases as we increase the value of "$1/k_BT$" for each sample and a similar trend was achieved for each sample. In previous section we discussed the variation of resistivity with temperature, where the resistivity was decreased with increase in temperature. The changes or variations occur in resistivity is mainly due to the drift mobility, higher the drift mobility lower will be the resistivity and vice versa. Fig 4.23 shows higher values of drift mobility at high values of temperature because the rate of hopping of charge carriers i.e. electrons increases with increase in temperature and in the result, it increases the drift mobility and decreases the resistivity. Similarly, the value of drift mobility also increased with increase in concentration of MWCNTs in $BaFe_{12}O_{19}$/MWCNTs nanocomposite due to the conductive nature and easy paths of conduction provided by MWCNTs. Fig 4.24 is showing the values of drift mobility at 298K for each sample. The values of drift mobility at 298K for each sample is given in Table 4.3

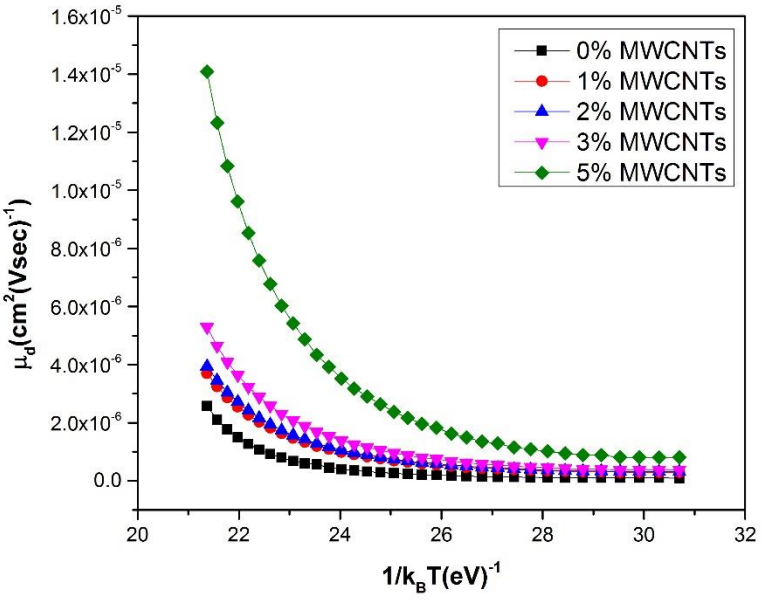

Fig 4.23 Temperature dependence of drift mobility (μ_d)

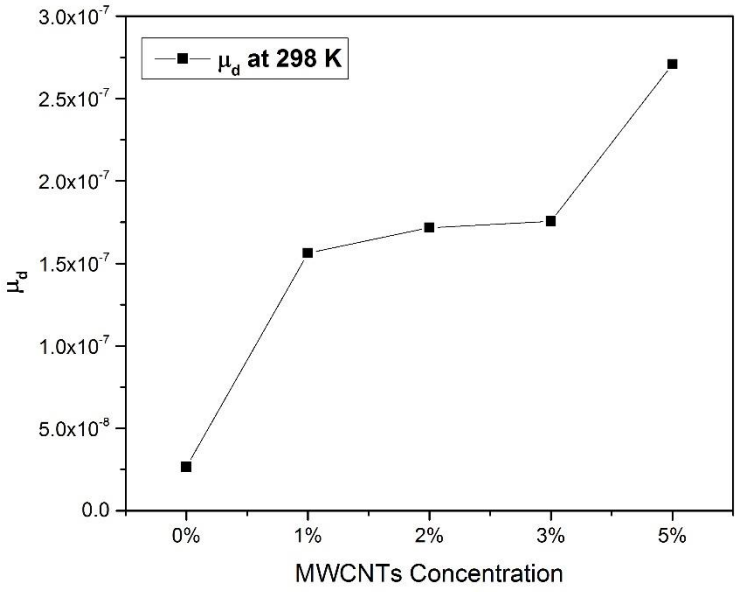

Fig 2.24 Values of drift mobility at 298 K.

Sample	ln ρ (Ω-cm) at 378 K	μ_d (cm^2/V. s) at 298 K
0% MWCNTs	12.60	2.66×10^{-8}
1% MWCNTs	11.45	1.56×10^{-7}
2% MWCNTs	11.37	1.71×10^{-7}
3% MWCNTs	11.08	1.75×10^{-7}
5% MWCNTs	10.45	2.70×10^{-7}

Table 4.3. Calculated values of dc resistivity at 378 K and drift mobility at 298K

(Chapter 5)

Conclusions and Proposed Future Work

5.1 Conclusion

1. For the synthesis of $BaFe_{12}O_{19}$ ferrite nanoparticles, chemical co-precipitation method has been used. The single phase of ferrites is confirmed with the help of X-ray diffractometer, with hexagonal structure for all samples.

2. For calculating average crystallite size Scherrer formula was used, and it is found in the range 30-35 nm.

3. The composite $BaFe_{12}O_{19}$/MWCNTs containing 1,2,3 and 5% by wt. MWCNTs has been prepared by ultrasonication method. The attachment of $BaFe_{12}O_{19}$ on the walls of MWCNTs was confirmed by the help of FTIR graphs and SEM. In FTIR graphs the vibrational bands were shifted to 442.12 and 607.09 cm^{-1} from 434.47 and 598.43 respectively. In SEM figures it is clear to see that the ferrite nanoparticles were evenly dispersed and no agglomeration was found.

4. The dielectric constant of all samples decreased with increasing in frequency and then after a certain point it became constant as it is reported in the literature. Moreover, the dielectric constant value increased as the wt% of MWCNTs was increased in the $BaFe_{12}O_{19}$/MWCNTs nanocomposite. The value of dielectric constant containing only $BaFe_{12}O_{19}$ and 0% MWCNTs is 6.4×10^2 which was increased to 2.0×10^3.

5. In case of dielectric loss, the plots for all sample followed the same pattern as dielectric constant i.e. decreased with increase in frequency. The dielectric loss increased as wt% of MWCNTs in $BaFe_{12}O_{19}$/MWCNTs nanocomposite was increased. The dielectric loss for only ferrite sample i.e. containing 0% MWCNTs 1.3×10^3 where the value of dielectric loss for the sample containing 5 wt% MWCNTs was 6.2×10^3.

6. The value of Tan loss also decreased with the increase in frequency and increase with increase in wt% of MWCNTs in $BaFe_{12}O_{19}$/MWCNTs nanocomposite.

7. The value of AC conductivity increased from 7.1×10^{-6} to 3.4×10^{-5} as wt% of MWCNTs increased from 0 to 5% in $BaFe_{12}O_{19}$/MWCNTs nanocomposite.

8. The impedance calculated for all samples found to be decreased with increase in frequency and as well as with increase in wt% of MWCNTs in $BaFe_{12}O_{19}$/MWCNTs nanocomposite. The impedance value decreased from 1.3×10^{8} to 3.5×10^{7} as the wt% of MWCNTs increased from 0 to 5%.

9. The electric modulus showed maximum values at higher frequencies, and shown decrease as we increased the wt% of MWCNTs in $BaFe_{12}O_{19}$/MWCNTs nanocomposite. The relaxation time increases with increase in wt% of MWCNTs.

10. The increase in temperature result in the decrease of resistivity. The drift mobility increased with increase in temperature and it decreased with increase in the wt% of MWCNTs in prepared samples.

5.2 Proposed Future Work

- Magnetic Properties of $BaFe_{12}O_{19}$/MWCNTs will be measured and studied.
- Different method of synthesis will be followed to increase the yield of product.
- Different dispersing medium will be used to attain better dispersions and attachment of nanoparticles for better results.
- The prepared nanocomposite will be used in some other matrices to study its properties, for example the prepared nanocomposite will be used in concrete to study its EMI shielding properties.

References

[1] S. Papp, I. Dékány, Growth of nearly monodisperse palladium nanoparticles on disaggregated kaolinite lamellae, in: I. Dékány (Ed.) Adsorption and Nanostructure, Springer Berlin Heidelberg, Berlin, Heidelberg, 2002, pp. 94-100.

[2] A. Aharoni, Introduction to the Theory of Ferromagnetism, Clarendon Press, 2000.

[3] J. Smit, H.P.J. Wijn, Ferrites: physical properties of ferrimagnetic oxides in relation to their technical applications, Wiley, 1959.

[4] P.N. Laboratorium, Philips Technical Review, Philips Research Laboratory., 1962.

[5] E.P. Wohlfarth, Preface, Handbook of Ferromagnetic Materials, vol Volume 3, Elsevier, 1982, pp. v-vi.

[6] H.-C. Cheng, C.-F. Chen, C.-Y. Tsay, J.-P. Leu, Journal of Alloys and Compounds 475 (2009) L46-L49.

[7] S.B. Narang, C. Singh, Y. Bai, I. Hudiara, Materials Chemistry and Physics 111 (2008) 225-231.

[8] B.C. Smith, Fundamentals of Fourier Transform Infrared Spectroscopy, CRC Press, 1995.

[9] N. Millot, S. Begin-Colin, P. Perriat, G. Le Caër, Journal of Solid State Chemistry 139 (1998) 66-78.

[10] M. Thackeray, M. Mansuetto, D. Dees, D. Vissers, Materials Research Bulletin 31 (1996) 133-140.

[11] H. Langbein, S. Christen, G. Bonsdorf, Thermochimica acta 327 (1999) 173-180.

[12] A. Shimada, M. Anzai, A. Kakuta, T. Kawanishi, IEEE transactions on industry applications (1987) 804-809.

[13] H.M. Hosseini, N. Naghibolashraphy, Journal of Alloys and Compounds 448 (2008) 284-286.

[14] W. Bragg, Nature 95 (1915) 561.

[15] J. Sláma, A. Grusková, M. Papánová, D. Kevická, R. Dosoudil, V. Jančárik, A. González, G. Mendoza, Journal of Magnetism and Magnetic Materials 272 (2004) 385-387.

[16] J. Smit, H.P.J. Wijn, (1959).

[17] H. Kojima, Handbook of Ferromagnetic Materials 3 (1982) 305-391.

[18] L. Lechevallier, J. Le Breton, A. Morel, P. Tenaud, Journal of Physics: Condensed Matter 20 (2008) 175203.

[19] M.J. Iqbal, M.N. Ashiq, Chemical Engineering Journal 136 (2008) 383-389.

[20] A. Goldman, Modern ferrite technology, Springer Science & Business Media, 2006.

[21] L. Wang, Q. Zhang, Journal of Alloys and Compounds 469 (2009) 251-257.

[22] E. Verwey, P. Haayman, F. Romeijn, The Journal of Chemical Physics 15 (1947) 181-187.

[23] M.J. Iqbal, S. Farooq, Materials Chemistry and Physics 118 (2009) 308-313.

[24] R.M. Almeida, W. Paraguassu, D.S. Pires, R.R. Corrêa, C.W. de Araujo Paschoal, Ceramics International 35 (2009) 2443-2447.

[25] M.N. Ashiq, M.J. Iqbal, I.H. Gul, Journal of Alloys and Compounds 487 (2009) 341-345.

[26] M.J. Iqbal, M.N. Ashiq, P. Hernandez-Gomez, J.M. Munoz, Journal of Magnetism and Magnetic Materials 320 (2008) 881-886.

[27] K.C. Kao, Dielectric phenomena in solids, Academic press, 2004.

[28] S. Pillai, New age international publishers, New Delhi (2005).

[29] W. Lixi, H. Qiang, M. Lei, Z. Qitu, Journal of Rare Earths 25 (2007) 216-219.

[30] P.C. Ma, B.Z. Tang, J.-K. Kim, Carbon 46 (2008) 1497-1505.

[31] Y. Konishi, M. Cakmak, Polymer 47 (2006) 5371-5391.

[32] P.-C. Ma, M.-Y. Liu, H. Zhang, S.-Q. Wang, R. Wang, K. Wang, Y.-K. Wong, B.-Z. Tang, S.-H. Hong, K.-W. Paik, ACS applied materials & interfaces 1 (2009) 1090-1096.

[33] V. Levchenko, Structure and electrophysical properties of nanocomposites based on thermoplastic polymers and carbon nanotubes, Université Claude Bernard-Lyon I, 2011.

[34] Y. Tang, Y. Hu, L. Song, R. Zong, Z. Gui, Z. Chen, W. Fan, Polymer Degradation and Stability 82 (2003) 127-131.

[35] Y.-Q. Zhang, J.-H. Lee, H.-J. Jang, C.-W. Nah, Composites Part B: Engineering 35 (2004) 133-138.

[36] V. Choudhary, B. Singh, R. Mathur, Carbon nanotubes and their composites, Syntheses and applications of carbon nanotubes and their composites, InTech, 2013.

[37] M.-F. Yu, B.S. Files, S. Arepalli, R.S. Ruoff, Physical review letters 84 (2000) 5552.

[38] M.-F. Yu, O. Lourie, M.J. Dyer, K. Moloni, T.F. Kelly, R.S. Ruoff, Science 287 (2000) 637-640.

[39] J.-O. Lee, C. Park, J.-J. Kim, J. Kim, J.W. Park, K.-H. Yoo, Journal of Physics D: Applied Physics 33 (2000) 1953.

[40] T. Ebbesen, H. Lezec, H. Hiura, J. Bennett, H. Ghaemi, T. Thio, Nature 382 (1996) 54-56.

[41] J.A. Schwarz, C.I. Contescu, K. Putyera, Dekker encyclopedia of nanoscience and nanotechnology, CRC press, 2004.

[42] M. Radwan, M. Rashad, M. Hessien, Journal of Materials Processing Technology 181 (2007) 106-109.

[43] M.N. Ashiq, M.J. Iqbal, I.H. Gul, Journal of Alloys and Compounds 487 (2009) 341-345.

[44] M. Javed Iqbal, M. Naeem Ashiq, I. Hussain Gul, Journal of Magnetism and Magnetic Materials 322 (2010) 1720-1726.

[45] A. Ghasemi, Journal of Magnetism and Magnetic Materials 323 (2011) 3133-3137.

[46] M. Jamalian, A. Ghasemi, E. Paimozd, Journal of Alloys and Compounds 604 (2014) 373-378.

[47] M.J. Iqbal, M.N. Ashiq, Scripta Materialia 56 (2007) 145-148.

[48] R. Jotania, R. Khomane, C. Chauhan, S. Menon, B. Kulkarni, Journal of Magnetism and Magnetic Materials 320 (2008) 1095-1101.

[49] C. Burda, X. Chen, R. Narayanan, M.A. El-Sayed, Chemical reviews 105 (2005) 1025-1102.

[50] T.T. Kodas, Advanced Materials 1 (1989) 180-192.

[51] V. Pillai, D. Shah, Journal of Magnetism and Magnetic Materials 163 (1996) 243-248.

[52] B.L. Cushing, V.L. Kolesnichenko, C.J. O'Connor, Chem Rev 104 (2004) 3893-3946.

[53] A.R. West, Basic solid state chemistry, John Wiley & Sons Inc, 1999.

[54] R.F. Egerton, The scanning electron microscope, Physical principles of electron microscopy, Springer, 2005, pp. 125-153.

[55] R.F. Egerton, Physical principles of electron microscopy, Springer, 2005.

[56] R.J. Bell, American Journal of Physics 41 (1973) 149-151.

[57] T. Theophanides, Introduction to infrared spectroscopy, Infrared Spectroscopy-Materials Science, Engineering and Technology, InTech, 2012.

[58] S. Chaudhury, S. Rakshit, S. Parida, Z. Singh, K.S. Mudher, V. Venugopal, Journal of Alloys and Compounds 455 (2008) 25-30.

[59] S. Farooq, Quaid-i-Azam University Islamabad, Pakistan (2010).

[60] R.D. Waldron, Physical Review 99 (1955) 1727-1735.

[61] N. Shiri, A. Amirabadizadeh, A. Ghasemi, Journal of Alloys and Compounds 690 (2017) 759-764.

[62] H. Li, C. Ra, G. Zhang, W.J. Yoo, J. Korean Phys. Soc 54 (2009) 1096-1099.

[63] I.H. Gul, A.Z. Abbasi, F. Amin, M. Anis-ur-Rehman, A. Maqsood, Journal of Magnetism and Magnetic Materials 311 (2007) 494-499.

[64] R.J. Pandya, U.S. Joshi, O.F. Caltun, Procedia Materials Science 10 (2015) 168-175.